Journal of
Sensor and Actuator Networks

MDPI

Review

A Review of Reconfigurable Intelligent Surfaces in Underwater Wireless Communication: Challenges and Future Directions

Tharuka Govinda Waduge [1,*], Yang Yang [1,2] and Boon-Chong Seet [1]

[1] Department of Electrical and Electronic Engineering, Auckland University of Technology, Auckland 1010, New Zealand; heu_yangyang@hotmail.com (Y.Y.); boon-chong.seet@aut.ac.nz (B.-C.S.)
[2] College of Underwater Acoustic Engineering, Harbin Engineering University, Harbin 150001, China
* Correspondence: tharukawaduge@gmail.com

Abstract

Underwater wireless communication (UWC) is an emerging technology crucial for automating marine industries, such as offshore aquaculture and energy production, and military applications. It is a key part of the 6G vision of creating a hyperconnected world for extending connectivity to the underwater environment. Of the three main practicable UWC technologies (acoustic, optical, and radiofrequency), acoustic methods are best for far-reaching links, while optical is best for high-bandwidth communication. Recently, utilizing reconfigurable intelligent surfaces (RISs) has become a hot topic in terrestrial applications, underscoring significant benefits for extending coverage, providing connectivity to blind spots, wireless power transmission, and more. However, the potential for further research works in underwater RIS is vast. Here, for the first time, we conduct an extensive survey of state-of-the-art of RIS and metasurfaces with a focus on underwater applications. Within a holistic perspective, this survey systematically evaluates acoustic, optical, and hybrid RIS, showing that environment-aware channel switching and joint communication architectures could deliver holistic gains over single-domain RIS in the distance–bandwidth trade-off, congestion mitigation, security, and energy efficiency. Additional focus is placed on the current challenges from research and realization perspectives. We discuss recent advances and suggest design considerations for coupling hybrid RIS with optical energy and piezoelectric acoustic energy harvesting, which along with distributed relaying, could realize self-sustainable underwater networks that are highly reliable, long-range, and high throughput. The most impactful future directions seem to be in applying RIS for enhancing underwater links in inhomogeneous environments and overcoming time-varying effects, realizing RIS hardware suitable for the underwater conditions, and achieving simultaneous transmission and reflection (STAR-RIS), and, particularly, in optical links—integrating the latest developments in metasurfaces.

Keywords: reconfigurable intelligent surfaces; underwater wireless communication; optical; acoustic; non-line-of-sight; inhomogeneous oceans

Academic Editors: Dionisis Kandris, Eleftherios Anastasiadis and Purav Shah

Received: 11 August 2025
Revised: 19 September 2025
Accepted: 19 September 2025
Published: 26 September 2025

Citation: Govinda Waduge, T.; Yang, Y.; Seet, B.-C. A Review of Reconfigurable Intelligent Surfaces in Underwater Wireless Communication: Challenges and Future Directions. *J. Sens. Actuator Netw.* **2025**, *14*, 97. https://doi.org/10.3390/jsan14050097

1. Introduction

The adoption of reconfigurable intelligent surfaces (RISs) has been discussed as a promising means of achieving telecommunication demands beyond 5G [1]. The use of RIS may be explained as the utilization of an intelligent or 'smart' intermediate node between the transmitter and receiver, which is fully able to configure reflective structures that redirect the incident signal to the receiver, either through active or passive means, achieving

an optimal signal reception than would the direct link. The RIS devices are often low-cost, highly efficient, and versatile, and deployable in mobile, sensor, and actuator networks [1]. A significant body of research is available for terrestrial implementations. However, it appears that RIS may also benefit underwater wireless communications (UWCs), an emergent research area in telecommunication, envisioned to be included with 6G technology.

Water has high conductivity and is, therefore, unsuitable for radiofrequency (RF) transmissions. The most feasible types researched for UWCs are optical and acoustic links, each with benefits competing with the other. Underwater optical wireless communication (UOWC) is established by transmitting photons in the visible-light spectrum. The speeds, bandwidths, and data rates are very high, with frequencies in the THz regime, and achieve low latencies, but are principally line-of-sight (LOS) links that are extinguished within tens of meters from high attenuation based on water clarity [2]. Underwater wireless acoustic communication (UWAC), on the other hand, propagates ultrasound waves. These can travel several kilometers and envelop around obstacles but are limited to frequencies of a few kHz and are affected by Doppler shifts and multipath receptions. Magnetic induction-based UWCs have also been explored but are comparatively less mature. The research to date suggests that RISs may be utilized to overcome the limitations of UOWCs and UWACs.

As shown in Figure 1, Applications of RISs for UWC may be classified by three configurations based on the location: stationery deployments on terrestrial structures on the shore or on the seabed; on floating RIS beneath the water surface, or on vehicular structures such as autonomous underwater vehicles (AUV) or on the hulls of surface vehicles (boats, buoys, etc.) [1]. The key benefit of stationery deployments is the consistency of the geometrical implications towards channel conditions. However, the rapidly time-varying nature of the underwater environment limits the synchronization and channel-estimation abilities of a link for ranges beyond a few hundred meters, which would limit the RIS from achieving its full potential. This effect would only exacerbate moving towards vehicular deployments, thus demanding robust and fast-responsive optimization strategies [1].

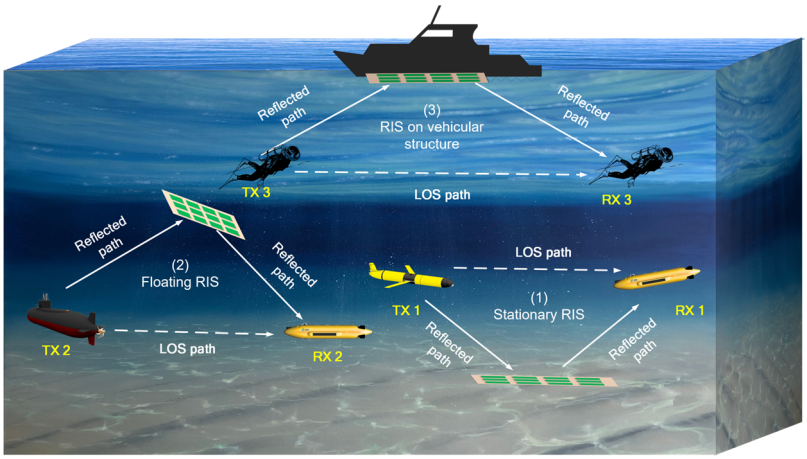

Figure 1. The three types of RIS-enabled underwater networks. Dashed and solid arrows show the LOS and RIS-based link paths, respectively.

To this end, we have surveyed both theoretical and physically developed state-of-the-art available to-date, in optical and acoustic RISs underwater. RF methods are discussed where they supplemented UWCs. Subsequently, we highlight the research challenges and gaps, and formulate directions for future research in areas such as hybrid acoustic and optical RIS networks, improved secrecy and security in inhomogeneous environments, opportunities in metasurfaces, etc.

This paper has been organized into the following sections:

1. **Introduction**: Introduces underwater wireless communication and RIS to the reader.
2. **Optical-RIS for UOWCs**: Surveys the existing O-RIS state-of-the-art from four perspectives—channel modeling of purely underwater O-RIS-based systems, and systems where RIS is above the water, but may have been used to assist a UOWC; towards enhancing physical layer security; enabling multiuser access, and finally, the works on metasurfaces for underwater applications that could potentially be adopted for O-RIS underwater.
3. **Acoustic-RIS for UWAC**: Surveys the existing A-RIS state-of-the-art from four perspectives—channel modeling of A-RIS-based systems, multiuser access, wideband beamforming, and hardware realizations.
4. **Research Challenges**: Key research challenges are discussed in terms of environmental and system-based challenges. The main environmental challenges relate to the inhomogeneity of the underwater medium and ambient noise, such as sunlight. System-level issues are discussed with a focus on secrecy and security, and multiuser access.
5. **Research Opportunities**: Opportunities for future works are discussed from the point of view of overcoming effects of inhomogeneity for optical and acoustic UWCs; incorporating more complex optical beam generation/conversion using metasurfaces and/or metalenses to achieve UOWCs more robust to occlusion effects; opportunities for incorporating deep-learning for the wideband beamforming of UWAs; multiuser links and resource allocation optimization in A-RIS; practical design and research considerations for realizing RIS hardware suitable for aquatic environments, and considerations towards realizing acoustic-optic hybrid RIS.
6. **Conclusions**: Concludes the article by packaging our main findings and making suggestions for future work.

2. Optical Reconfigurable Intelligent Surfaces (O-RIS) for UOWCs

Visible light communication (VLC) based Light-Fidelity (LiFi) is identified as a cutting-edge technological paradigm integral to future terrestrial 6G systems [3]. However, the reliability of the VLC link reception is contingent on a line-of-sight path and favorable environmental conditions, which may be challenging to attain, especially in dynamic communication systems such as mobile links. The benefits of RIS are highlighted in such applications, where it allows a cost- and power-efficient way to fully control and customize the physical propagation [3].

RIS for VLCs differentiate from radiofrequency (RF) based deployments, particularly utilizing intensity-modulation and direct-detection (IMDD) schemes for transmitting real, non-negative signals that need to optimize illumination and communication simultaneously [4]. From a hardware perspective, optical RIS may come as mirror arrays or metasurfaces. Mirror arrays capitalize on Snell's laws of reflection to change the orientations of planar mirror elements [5]. On the contrary, metasurfaces rely on uniquely engineered planar surfaces of "meta-atoms" that are capable of dynamically altering their dielectric properties, permeability, permittivity, and refractive index [3,5,6]. These allow greater manipulation of the outgoing photons through refractive index tuning and anomalous reflections, where the relationship between the angle of incidence and reflection (Snell's law) can be broken to even "bend" the direction, amplify, attenuate, or completely absorb signals, or even control wavelengths independently [3,6–10]. However, overall, metasurfaces may be better for compact setups and dynamic control of the beams, while reflector arrays are advantageous for wider coverage [11].

RIS for terrestrial free-space-optical (FSO) communication has been comprehensively surveyed. Nonetheless, transitioning to underwater media, which exhibits more complex and diverse spatial characteristics than air, demands dedicated attention. Thus, in the following sections, we aim to comprehensively survey the research to date on RIS from a UOWC perspective.

2.1. Channel Modeling (O-RIS)

Naik and Chung conduct one of the first parameter-dependent analytical studies for RIS performance underwater, deriving closed-form equations for the bit-error rate (BER), channel capacity, and outage probability (OP) [12]. Their performance outcomes for an RIS-based UOWC system are compared comprehensively against a direct link for many parameter combinations, such as the influence of weak and strong pointing errors, IMDD and heterodyne light detection, coherent and non-coherent modulation forms of binary-phase-shift-keying (BPSK) and binary-frequency-shift-keying (BFSK), turbulence and attenuation, and different blocking probabilities. Overall, the results indicate that the RIS-assisted system outperforms the direct link when those physical parameters are varied and is improved further with a higher number of RIS elements. Coherent detection outperforms non-coherent detection by about 4 dB, and heterodyne detection allows for a greater channel capacity. Here, the probability density function the authors use for turbulence is from the generalized Gamma function for a plane wave, incorporating the Oceanic Turbulence Optical Power Spectrum (OTOPS) model to determine the power spectrum based on preselected salinity and temperature values. Their work was validated through a Monte Carlo simulation. Ata et al. conduct a similar numerical analysis using a log-normal distribution for turbulence with OTOPS, considering both for a plane-wave and a Gaussian beam [13]. Here, the authors use a beam-attenuation coefficient model developed by Haltrin, which is based on the concentration of chlorophyll-a (Chl-a) in the water, a primary pigment constituent of phytoplankton and other photosynthetic organisms [14]. Their work explores the effect of water type, link length, receiver aperture diameter, temperature, and energy dissipation rates (two key parameters that govern turbulence), reflection coefficient of the RIS, and beam waist towards the outage probability of non-RIS and RIS-based systems of 100, 500, and 1000 elements. Overall, the RIS-assisted links perform better than the non-RIS system, further showing that higher reflection coefficients, bigger receiver apertures and transmitter beam waists, and clearer waters may improve the performance. The performance was better with lower temperature dissipation rates but a higher energy dissipation rate of the water, both indicative of lower turbulent environments. Their results seem to suggest that the improvement of the RIS-based system could saturate at a high number of RIS elements. Regarding misalignments and non-zero boresight pointing errors of Gaussian beams, it appears that the transmitted power is a key factor for bit rates over 500 kbps [15]. However, this may be mitigated by generating higher-order mode beams with asymmetric beam deviations, particularly in weak to moderate turbulence regimes [16]. Salam et al. supplements these works by investigating how an optical intelligent reflecting surface (OIRS) configuration may compare to a planar (fixed) mirror-array surface (PMS), and to non-line-of-sight (NLOS) reflections at the air-water interface by total-internal-reflection (TIR) [17]. They model the reception with a silicon photomultiplier (SiPM), which is an array of single-photon avalanche diodes (SPADs) operating in Geiger mode. (This is when the avalanche-photodiodes are biased slightly above the breakdown voltage, such that a single-photon incidence can create an avalanche effect). The results show that the OIRS performed the best under most accounts, such as increasing node separation and decreasing transmit power. However, the energy efficiency of the OIRS decreases as the number of reflecting elements increases, because energy utilization has

increased even though the spectral efficiency reaches saturation, suggesting that the OIRS array size needs to be selected with the end goal in mind. However, a key critique of the use of the air–water interface is that the possibility of waves has not been accounted for. The analysis is numerical and is validated by a Monte Carlo simulation. However, in contrast to all the above analyses where numerical methods took precedence, a fully Monte-Carlo-based study for RIS-assisted links in coastal and harbor waters showed that the effect of the high scattering possibly increases the probability of photons reaching the receiver from both the LOS path and the reflected one [18]. This is exacerbated with increased link distance and thus, may be a cause of interference. Therefore, given that this can be traced back to the Chl-a content of the water, which is measurable by sensors, it may be wise to design the RIS-assisted UOWC system accordingly [16]. However, concerning single-input multiple-output (SIMO) impulse responsiveness in coastal waters, RISs that use active beam steering seem to perform much better compared to just specular reflections, especially considering those receivers not within LOS of the transmitter. They show a narrower temporal response leading to lower inter-symbol interference (ISI), BER, and a wider 3-dB bandwidth [19]. RIS has also been explored towards mitigating UOWC occlusions due to sea mounts, marine life, and underwater equipment [20]. In such applications, at low SNR, the finite-SNR diversity order would increase with a greater number of elements, observed for 2, 4, 8, and 12 reflecting elements. However, at high SNR, the diversity order appears to not change significantly. Figure 2 depicts the characteristics of the main reflection-based UOWCs discussed.

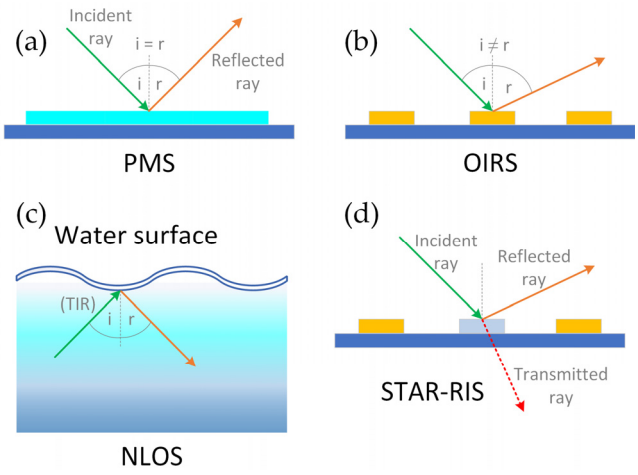

Figure 2. A depiction of the different reflection types discussed for UOWCs. The green arrows show the incident rays, and the orange arrows show the reflected rays (**a**) When using passive mirrors, the angle of reflection, r, will be identical to the angle of incidence, i. (**b**) In OIRS, beam steering allows a greater level of control over the reflected path. This could be achieved with RIS elements mounted on actuators, or by dynamic adjustment of dielectric properties of meta-elements. (**c**) NLOS paths may be achieved also using sea surface for TIR. (**d**) Simultaneously transmitting and reflecting (STAR) RISs can extend connectivity to both half-spaces on opposing sides. The red dashed arrows show transmitted rays.

Some of the key metrics discussed can be summarized in Tables 1–4. Here, L is distance in m; χ_T is the temperature dissipation rate; ϵ is the kinetic energy dissipation rate; α and β are large- and small-scale turbulent eddies; λ is the wavelength; $\langle T \rangle$ is the average temperature in °C; $\langle S \rangle$ is the average salinity in PSU; c is the attenuation coefficient; H is the temperature-salinity gradient ratio; D_G is the aperture diameter; W_0 is the beam radius; F_0 is the phase front radius; $\overline{\gamma}$ is the average SNR; N is the number of RIS elements; β_r is the reflection coefficient; C_c is the chlorophyll concentration; σ_s is the standard deviation of pointing error; a_0 is the mirror array area; σ_I^2 is the scintillation index.

Table 1. Comparisons of coherent and non-coherent BPSK and BFSK modulation, and IMDD and HD detection schemes, for a LOS link and RIS-based links. Two RIS links are considered—where channel fading is independently and identically distributed (i.i.d.), and independent and non-identically distributed (i.ni.d). Turbulence modeled by a generalized Gamma model [12].

Fixed Parameters (If Not Stated)	**Metric**	**LOS Link**	**i.i.d RIS Link (N = 1/4/16)**	**i.ni.d RIS Link (N = 1/4/16)**	**Observations**
Plane wave, λ = 470 nm, c = 0.056 m^{-1}	When BER = 10^{-5} (BPSK coherent)	SNR = ~93 dB	SNR = 49/46/43 dB	SNR = 33/28/18 dB	Coherent ~2–3 dB better than non-coherent
Direct Link: L = 100 m, $\epsilon = 10^{-6}$ m^2/s^3, $\chi_T = 10^{-2}$ K^2/s, α = 2.01	When BER = 10^{-5} (BFSK coherent)	SNR = ~96 dB	SNR = 46.5 dB (N = 16)	SNR = 20 dB (N = 16)	Coherent ~2–3 dB better than non-coherent
Source to RIS: L = 50 m, $\epsilon = 10^{-8}$ m^2/s^3, $\chi_T = 10^{-3}$ K^2/s, α = 57.32	When OP = 2 × 10^{-5} at threshold SNR of 5 dB	SNR = ~100 dB	SNR = 57.5/54.5/ 51.5 dB	SNR = 41/36/25 dB	$N \times 4 \rightarrow$ ~2 dB (i.i.d) or ≥6 dB (i.ni.d) gain, for given OP.
RIS to destination: L = 100 m, $\epsilon = 10^{-8}$ m^2/s^3, $\chi_T = 10^{-2}$ K^2/s, β = 1.31	Channel capacity (CC)	For CC ~17 bits/s/Hz: IM/DD: ~60 dB; HD: ~56 dB SNR	~30 dB SNR gain (N = 4); ~50 dB gain (N = 16) compared to N = 1, for CC at 18 bits/s/Hz	~5 dB SNR gain (N = 4); ~15 dB SNR gain (N = 16) compared to N = 1, for CC at 4 bits/s/Hz.	HD ~4 dB better than IMDD for all cases.

Table 2. Comparison between LOS and RIS-based UOWC performances under scaled temperature (χ_T) and energy dissipation (ϵ) factors in log-normal turbulence, and varied water types [13].

Fixed Parameters (If Not Stated)	**Parameter Change**	**Conditions**	**Outage Probability**
Plane wave, λ = 470 nm $\langle T \rangle$ = 15 °C $\langle S \rangle$ = 20 ppt $\epsilon = 10^{-5}$ m^2/s^3 $\chi_T = 10^{-2}$ K^2/s H = −2 °C/ppt D_G = 2 cm W_0 = 2 cm $F_0 = \infty$ $\overline{\gamma}$ = 40 dB N = 50 β_r = 1 C_c = 0.03 mg/m^3 $\sigma_s = 3 \times 0.5 D_G$ L = 20 m	Temperature dissipation rate χ_T ($10^{-10} \rightarrow 10^{-4}$ K^2/s)	N = 0 (No RIS, LOS) N = 100 N = 500 N = 1000	$7 \times 10^{-4} \rightarrow 3 \times 10^{-1}$ $2 \times 10^{-6} \rightarrow 8 \times 10^{-4}$ $3 \times 10^{-7} \rightarrow 1 \times 10^{-4}$ $1 \times 10^{-7} \rightarrow 4 \times 10^{-5}$ (reaches saturation with higher N)
	Energy dissipation rate ε ($10^{-10} \rightarrow 10^{-2}$ m^2/s^3)	N = 0 (No RIS, LOS) N = 100 N = 500 N = 1000	$1.5 \rightarrow 7 \times 10^{-3}$ $4 \times 10^{-4} \rightarrow 2 \times 10^{-5}$ $5 \times 10^{-5} \rightarrow 2.5 \times 10^{-6}$ $2 \times 10^{-5} \rightarrow 1 \times 10^{-6}$ (reaches saturation with higher N)
	Link length L (10 → 40 m)	D_G = 2 cm, N = 50	$2.4 \times 10^{-5} \rightarrow 2.6 \times 10^{-3}$
	IRS scaling at L = 20 m	N: 0 → 100 → 500 → 1000	$2.4 \times 10^{-2} \rightarrow 6.5 \times 10^{-5} \rightarrow 8.3 \times 10^{-6} \rightarrow 3.4 \times 10^{-6}$
	Receiver aperture D_G (0 → 2 cm)	$N \geq 100$	~ D_G = 2 cm is 3 times better than a 0 cm point receiver
	Water type (absorption/scattering)	N = 50, L = 10 m	At OP ≈ 10^{-4}, SNR is: Pure water: 32 dB Clear ocean: 36 dB Coastal ocean: 42 dB Harbor: 61 dB

Table 3. Impulse response comparison between LOS and RIS-enabled SIMO in coastal waters. Results shown for RIS with specular reflection and beam-steering [19].

Fixed Parameters	Metric	Condition	LOS (No RIS)	RIS–Specular Reflection	RIS–Beam Steering
λ = blue-green band c = 0.305 m^{-1} (coastal water) 10° emission divergence 10° receiver field-of-view 50 cm aperture 102 × 100 RIS array 0.01 × 0.01 m^2 element size	Temporal dispersion (10 m link)	Peak width at –20 dB	Approx. 0.550 ns	Approx. 0.425 ns	Approx. 0.162 ns
	Temporal dispersion (20 m link)	Peak width at –20 dB	Approx. 0.788 ns	Approx. 0.600 ns	Approx. 0.325 ns
	3-dB Bandwidth (10 m link)	Relative to LOS	Baseline	~0.7 × higher	~1.3 × higher
	3-dB Bandwidth (20 m link)	Relative to LOS	Baseline	~0.5 × higher	~1.5 × higher
	BER (10 m, 1 Gbps OOK)	SNR = 0 dB	~10^{-1}	~<10^{-8}	<10^{-8}
	BER (20 m, 1 Gbps OOK)	SNR = 15 dB	~8 × 10^{-2}	~10^{-5}	<10^{-8}

Table 4. A comparison of spectral efficiency, energy efficiency, outage probability and BER for passive-mirror surface, RIS, and reflection at water-air interface (NLOS) under weak to moderate turbulence [17]. Turbulence is modeled using the exponentiated Weibull distribution.

Metric	Turbulence	OIRS	PMS	NLOS	OIRS Advantage over PMS
Spectral Efficiency (bits/s/Hz)	Weak (σ_I^2 = 0.2178)	~15	~7.5	~6.5	~2.00
	Moderate (σ_I^2 = 1.9328)	~12	~5.5	~4	~2.18
Energy Efficiency (10 W transmit power)	-	a_0 = 1 m^2 → 0.48 a_0 = 4 m^2 → 0.6 a_0 = 9 m^2 → 0.67 a_0 = 16 m^2 → 0.74	0.51	0.45	a_0 = 1 m^2 → ~0.94 a_0 = 4 m^2 → ~1.18 a_0 = 9 m^2 → ~1.31 a_0 = 16 m^2 → ~1.45
Outage Probability	Weak (σ_I^2 = 0.2178)	~10^{-2}	~1.2 × 10^{-1}	~1.5 × 10^{-1}	~12
	Moderate (σ_I^2 = 1.9328)	~6.5 × 10^{-2}	~5.5 × 10^{-1}	~7.5 × 10^{-1}	~8.5
BER	Weak (σ_I^2 = 0.2178)	~2 × 10^{-3}	~2 × 10^{-2}	~3 × 10^{-2}	~10
	Moderate (σ_I^2 = 1.9328)	~7 × 10^{-3}	~7.5 × 10^{-2}	~2 × 10^{-1}	~11

In designing O-RIS-assisted networks, it would also be useful to know the required number of RIS elements for different ocean environments, such as in terms of the water types, or at the depths of interest in inhomogeneous water columns. Unfortunately, this information is not directly available from the surveyed works but may be inferred based on the available results. In pure and clear ocean waters (Jerlov I–II), where scattering and absorption are minimal, only a moderate number of RIS elements (100–200) may be sufficient, since performance gains tend to saturate quickly and energy efficiency declines beyond this range. As water conditions worsen, larger RIS arrays of about 200–500 elements are necessary to counteract moderate attenuation and turbulence, though improvements begin to level off beyond 500 elements. In coastal waters (Jerlov III and C-types), where

scattering and multipath effects are more pronounced, higher counts of 500–800 elements may be useful to maintain SNR diversity and suppress ISI. Finally, in harbor or highly turbid waters (Jerlov 7C, 9C), arrays of 800–1000 elements may improve the performance under very low SNR conditions, but the benefits are expected to be incremental and plateau rapidly, making it more practical to pair RIS with relays or diversity schemes (multihop relays, DF, AF, MIMO, etc.) rather than relying on RIS alone. Further investigations should be conducted to uncover more accurately the performance outcomes of scaling RIS under different water types and other oceanic environmental factors.

In addition to RIS underwater, works are also available where UOWCs were integrated into a RIS-based relay system connecting terrestrial and underwater environments, where at least one RIS array was positioned above the water. The channel modeling includes common performance metrics such as outage probability, SNR, spectral efficiency and capacity, and BER analyses. Here, we summarize the main contributions that can be categorized firstly by relaying scheme, and thereafter, the modulation schemes used.

Odeyemi et al. first explored a decode-and-forward (DF) relaying protocol for a terrestrial RF-RIS link that starts as a UOWC from an underwater node, linked to an intermediate node stationed on the sea surface [21]. Closed-form expressions are provided for the outage probability and bit-error-rates incorporating turbulent UOWC channel conditions under unified effect from both bubbles, temperature and salinity [22]. The results follow the previously discussed assessments that heterodyne detection outperforms IMDD, that more RIS elements improve gain, and that BPSK is better than BFSK. A similar dual-hop RIS-based terrestrial RF to UOWC relaying is explored for comparisons between DF and a fixed-gain amplify-and-forward (AF) scheme employed at a marine buoy [23]. The terrestrial source-to-RIS link is modeled by a Nakagami-m distribution with Rayleigh fading. The results show that for higher m (shape parameter) values and reflecting RIS elements, the link performance is mainly governed by the UOWC channel conditions. The channel capacity is slightly improved for fresh water compared to salty water, and the outage probability of the AF scheme significantly outperforms DF with g higher signal-to-noise-ratio (SNR). The work by Salam et al. further compares performances for a dual-hop link where, due to a blockage between the base-station and the marine buoy, a terrestrial hop employs a RIS-based system and DF relaying [24]. The DF relay underperforms the RIS system when the RIS elements are high, about 100, but outperforms at smaller element numbers, like 20. For a low element number, the spectrum efficiently improved with higher transmission power. Conversely, it can be argued that DF-relay is more energy efficient compared to a RIS with fewer elements. The spectral efficiency of the IRS system was higher with shorter relay distances, overall, and for a given distance between the base station and buoy, peaked at the halfway point.

A triple-hop scheme (RF-RIS-RF to FSO-RIS-FSO to UOWC) is explored under different modulation schemes: differential binary phase shift keying (DBPSK), non-coherent binary phase shift keying (NCBPSK), coherent binary phase shift keying (CBPSK), and coherent binary frequency shift keying (CBFSK) [25]. Overall, CBPSK showed superior average BER performance compared to other schemes. A dual-hop FSO and UOWC relay system was further studied for the benefits of integrating RIS [26]. It uses an infrared FSO at 1550 nm and a UOWC at 530 nm. They model the effects of the system under weak, moderate, and strong skip-zones due to occlusions and blockage, providing the closed-form equations for SNR, outage probability, and BER. CBPSK, once again, outperforms the other modulation schemes of NCBPSK, CBFSK, and non-coherent binary frequency shift keying (NCBFSK), with RIS-assisted links outperforming the direct link under occlusions. In a similar thread, a THz (RF) to UOWC, RIS-based relay system has been investigated using an $\alpha - \mu$ distribution, with similar performance improvements when using the RIS

system and under pointing errors, turbulence, and bubbles. CBPSK performed better than CBFSK and non-binary PSK [27]. The RIS may also be used as a high-altitude platform station (HAPS)-based dual-hop relay to mitigate occlusions on the ocean surface. Deka et al. derive the analytical expressions for outage probability, BER, and SNR for such an application, and show that for such schemes using FSO and UOWCs, the orientation of the HAPS and the optical beam waist are key parameters to maintaining link performance [28]. CBPSK outperformed NCBFSK here. Table 5 summarizes these works, and Figure 3 illustrates the different systems discussed.

Table 5. A summary of the different contributions for RIS-assisted terrestrial RF and/or FSO systems with integrated UOWC.

Reference	Key Contributions
Odeyemi et al. [21]	• A dual-hop UWOC/RF RIS-assisted relay system. • RIS is above water for RF link. • Compares HD and IM/DD detection. • DF scheme is employed at a surface vehicle.
Li et al. [23]	• A or a dual-hop UWOC/RF RIS-assisted system. • RIS is above water for RF link. • Compares HD and IM/DD detection. AF and DF schemes are employed at a marine buoy.
Salam et al. [24]	• A comparative framework for IRS- and DF relay-assisted mixed RF-UWOC systems • Provides results for energy efficiency. • RIS is above water for RF link.
Elsayed et al. [29]	• NOMA-based RIS-assisted dual-hop RF-UOWC system. • RIS is above water for RF link.
Kumar et al. [25]	• Triple hop link with RF-RIS-RF, FSO-RIS-RF to UOWC. • Performance assessments for DBPSK, CBPSK, CBFSK, and NCBFSK modulation schemes.
Ramavath et al. [26]	• Dual-hop system with FSO and UOWC. • RIS is both above and below water. • Assesses performance in the presence of skip zones (regions of optical loss due to increased activity of plants, trees, seamounts, vehicles, fish, etc.).
Deka et al. [28]	• RIS-based HAPS assisted FSO-UOWC system. • RIS is at a high-altitude.
Rakib et al. [27]	• Dual-hop THz-UOWC terrestrial-to-underwater system. • Both the THz-RIS and UOWC-RIS are above water. • Performance assessments for DBPSK, CBPSK, CBFSK, and NCBFSK modulation schemes.

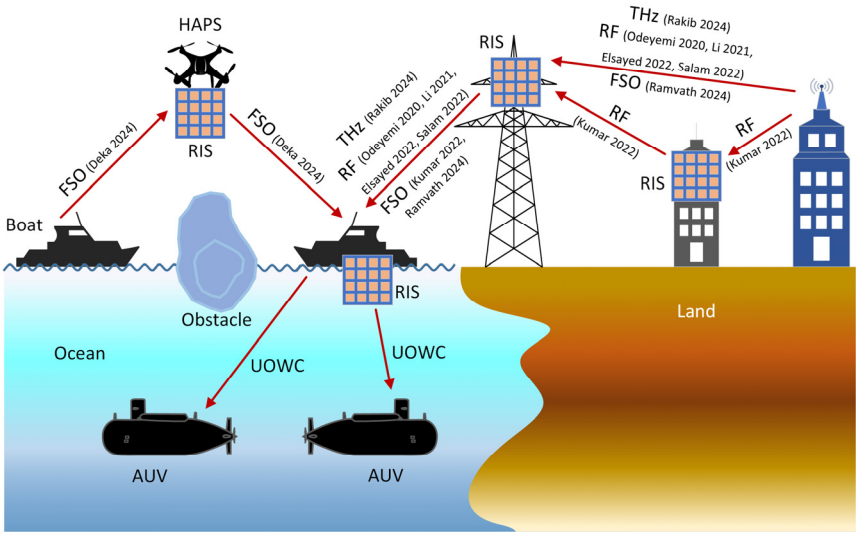

Figure 3. An illustration of the various types of RIS-assisted relays that support UOWCs. The arrows depict the connection strategy and direction discussed in each of the given works [21,23–29].

2.2. Physical Layer Security Improvement

Security of the physical layer has been a critical issue under investigation for the development of high-yielding 5G and 6G technologies. The earliest study on this regard for a RIS-aided system was conducted for an RF-UOWC hybrid network, observing the probability of interception by an eavesdropper [30]. The observations are made for heterodyne and IMDD optical signal detection for varied salinity and temperature gradients and bubble levels, for RIS arrays stationed above water. The turbulence model is a mixture-exponential generalized Gamma (mEGG) distribution. The average secrecy capacity (ASC), secrecy outage probability (SOP), strictly positive secrecy capacity (SPSC), and effective secrecy throughput (EST) are analyzed, showing that performance degrades in seawater (compared to freshwater) with turbulence gradients and high bubble levels, and improves with higher element numbers. However, the caveat is that the eavesdropper is a terrestrial one, listening on the RF link, and not much insight can be gained regarding the eavesdropping of the UOWC link.

A more targeted analysis is available in Sarawar et al. where an unmanned aerial vehicle (UAV) connects to an underwater destination through a dual-hop, RF to UOWC configuration, with an underwater RIS as an intermediary [31]. The system involves two eavesdroppers, one above water (RF) and one below (UOWC). The one below listens on the RIS-reflected UOWC channel. The ASC, SOP, SPSC, and EST are determined analytically. The secrecy performance of the underwater portion degrades with higher attenuation coefficient, salinity and temperature gradients, and the presence of bubbles, as in the previous analyses. Turbulence model is a mEGG distribution. Overall, the authors highlight for the RF portion, the link should be optimized for the fading severity parameters, that the small-scale fading parameters need to be well understood for an optimal balance between the total fading and the purposeful utilization of multipaths, and that link distances should be strategic to avoid both interception (if too short) and interference (if too long). The UOWC portion seems to improve under conditions highlighted in Section 2.1. A similar scenario is observed under a log-normal turbulence distribution by Sy et al. [32]. Supplementary to previous works, they show that as the link distance increases, the minimum separation between the destination and the eavesdropper should also increase. For example, to achieve an SOP of 10^{-6}, the separation between the legitimate receiver and eavesdropper under stronger turbulence should be 0.15 m, while this increases to 0.4 m for a 100 m link. This does depend heavily on the transmission parameters. However, comparing this distance to the expanse of the ocean and the probability of an eavesdropper being so proximate, it appears rather secure. Additionally, the secrecy throughput, for a given target secrecy rate is highly dependent on the turbulence strength. For example, when the turbulence strength is 10^{-11}, and the target secrecy rate is 0.6, the secrecy throughputs when the eavesdropper and intended user are 1 m and 2 m apart, are ~0.6, for both. However, for the same target secrecy rate, at a higher turbulence strength of 10^{-10}, the throughputs are approximately 0.25 and 0.5, for separations of 1 m and 2 m.

In light of these developments, Tian and Zheng evaluate the potential for using a security-based adaptive RIS (SA-RIS) clustering strategy in a multihop RIS-assisted UOWC system, where optical signals are reflected among clusters to improve the security [33]. The UOWC system is modeled in a weak turbulence environment modeled by a Gamma-Gamma distribution (Rytov variance, σ_l^2 at $0.2-0.6$), for a source wavelength at 532 nm due to the least absorption and scattering, with the number of reflecting elements at 15. Three scenarios were studied. The first, which fails to evade the eavesdropper, where the destination node and eavesdropper share the channel without a RIS-selection strategy (F-evasion); second, a mere RIS-clustering strategy without screening (N-selection), and the final, where channel qualities are screened and assigned to maximize the destination's

receive SNR (S-assign). S-assign outperforms the other schemes. For example, to achieve an SOP of 5×10^{-1} F-evasion and N-selection requires an SNR of 150 dB and 130 dB, respectively (propagation loss factor 10^{-4}) and S-assign only requires an SNR of approx. 30 dB even at a higher propagation loss factor of 10^{-3}. Comparing the ASC between the schemes, S-assign outperforms N-Selection by a 100% or more at all SNR. Higher number of RIS clusters tends to decrease the ASC with a constant attenuation coefficient, due to an increase in the distance between. However, the ASC converges at high SNR for a very low number of RIS clusters, which improves with more RIS clusters, so an optimal balance would need to be reached. Table 6 summarizes these works.

Table 6. A summary of the contributions from different works assessing the physical layer security aspects of RIS-assisted UOWCs.

Reference	Key Contributions
Hossain et al. [30]	• Secrecy performance analysis investigated for RIS-aided dual-hop RF-UOWC system incorporating the Nakagami-m distribution for RF links and the mixture exponential generalized Gamma (mEGG) model for UOWC links. • ASC, SOP, SPSC, and EST are analyzed under the effects of temperature gradients, air bubbles, with IM/DD and HD detection techniques. • RIS and eavesdroppers are above the water.
Sarawar et al. [31]	• Introduces a UAV-based RF-UOWC system with an underwater RIS, modeling simultaneous eavesdropping on both RF and UOWC links. • ASC, SOP, SPSC, and EST are analyzed with an optical link experiencing varied turbulence, pointing errors, and fading parameters. • Turbulence model is the mEGG distribution.
Sy et al. [32]	• An IRS-assisted UOWC system incorporating impairments where IRS is completely below the water. • SOP and secrecy throughput are analyzed under varied oceanic turbulence, propagation loss, and geometric misalignment, and the distance between legitimate users and eavesdroppers. • Turbulence is a significant factor affecting secrecy throughput for a given target secrecy rate. • The turbulence model is a log-normal distribution.
Tian and Zheng [33]	• A multihop RIS-assisted UOWC integrating SA-RIS clustering strategies to enhance physical layer security, showing promising results. • The novel scheme proposed outperforms the conventional scheme by over 100% across all SNR. • ASC of smaller clusters are better at low SNR but saturates at high SNR. Thus, larger clusters are recommended at high SNR. • The turbulence model is a Gamma-Gamma distribution.

2.3. RIS-Assisted Multiuser Strategies

The application strategies involving RIS multiuser communication are being developed. Given the change of medium, although terrestrial strategies can be translated, they need to be purposefully designed. An OIRS, by design, is fundamentally meant to support multiple users by dynamically grouping and allocating reflector elements based on the channel state information [34]. Salam et al. explore equal mirror assignment (EMA) and distance-based mirror assignment (DMA) against conventional orthogonal multiple access (OMA), non-orthogonal multiple access (NOMA), and rate-split multiple access (RSMA) as a means of improving aggregate spectral efficiency (ASE) and preserving user fairness [34]. The performance variations are analyzed against ocean depth as well for clear, open oceanic and coastal stratification conditions S1 and S8, respectively [35]. The results show that for ASE with N of six users, DMA performs the best, followed by EMA. OMA is better than NOMA and RSMA at low transmit power, due to NOMA and RSMA-based users experiencing interference from simultaneous transmissions. However, with

increasing transmit power, RSMA appears more spectrally efficient than both NOMA and OMA. With a fixed transmit power of 37 dBm and 16 OIRS elements of 16, DMA is still showing superior spectral efficiency than EMA, OMA, NOMA, and RSMA, with increasing aggregate number of users. With respect to the fairness index, OMA appears to be the best, closely followed by DMA, EMA, and RSMA, with NOMA showing the worst performance with an increasing number of users. DMA, appearing as the more suitable scheme, is further analyzed under turbulence and pointing errors, and attenuation, showing worsening performance under increasing effects. Thereafter, the performance vs. depth is observed. However, we deem these adopted coefficients doubtful, as explained in Waduge et al. [36], where the coefficients have been revised. For example, it is unlikely that a coastal S8-type environment could be 450 m deep [36]. For the ease of the reader, we have summarized the details regarding oceanic stratification under Section 4.1.1 and have subsequently provided the equations and coefficients. Alternatively, the underwater deployment of a simultaneous transmit and reflect (STAR)-RIS system has also been analyzed by Naik et al. [37]. The uniqueness of a STAR-RIS over the conventional RIS is its ability to transmit or direct the oncoming beam into the opposite half-space, a key requirement for underwater deployments. This capability would offer expanded degrees of freedom for controlling signal propagation, substantially enhancing design flexibility to meet stringent communication requirements. Benea-Chelmus et al. [38] demonstrated the first optical STAR-RIS using a two-state electro-optical plasmonic metamaterial surface. They achieved this by combining two anisotropic materials, liquid crystal and terthiophene, enabling precise control over the direction of reflected and transmitted beams. Details of a liquid-crystal-based RIS and optical beam transmission using terthiophene are available in Ndjiongue et al. and Matsuo et al., respectively [8,39]. In the underwater system, the STAR-RIS shows a two-fold improvement of received luminous intensity at the receiver, possibly due to it being an intermediate node that focuses the beam compared to the direct, LOS link, which continuously diverges with propagation [37]. Analytical results show that STAR-RIS achieves 5×10^{-4} BER at 26 dB, while the five-element RIS does so at 32 dB compared to the direct link at 68 dB. The STAR-RIS showed significant improvement in outage performance compared to the direct link, for both IMDD and heterodyne schemes. Channel capacity is also higher due to obtaining the strongest signal with the increased number of transmit-reflect elements over the direct UWOC link and full-space coverage over the regular RIS, which provides coverage to one half-space. Lastly, similar to works discussed in the previous sections, heterodyne detection of BPSK showed the best BER performance, followed by HD BFSK, and then IMDD OOK and 16-QAM. Finally, a completely unique implementation is proposed by AbdElKader et al., where a RIS-assisted modulating retroreflector (MRR) system employs the spectral-power-efficient L-ary Quadrature Amplitude Modulation Multipulse Pulse-Position Modulation (LQAM-MPPM) [40]. An MRR is usually made with an external light modulator and a passive reflector. It operates by encoding the data onto the incoming light signal, which is then reflected to the destination. Results comparing 4QAM-MPPM to MPPM, and 8QAM-MPPM to 4QAM show that the BER and power-efficiency of L-QAM-MPPM is better than the conventional case in attenuation, turbulence, and pointing error conditions. This was further improved with a greater number of RIS elements, but it is particularly contingent on where the RIS is placed between the transmitter and the MRR. Figure 4 illustrates the strategy.

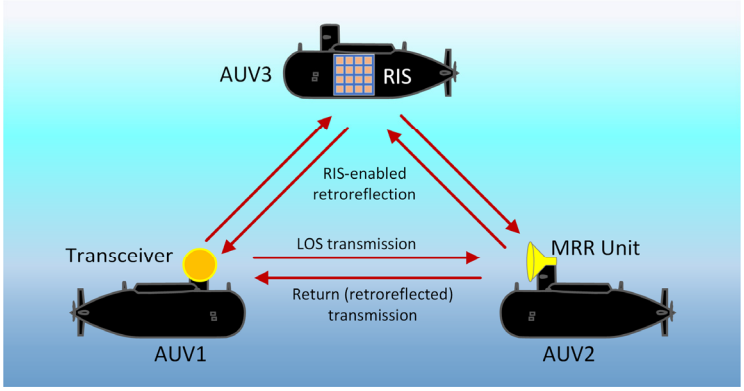

Figure 4. An illustration of the system model by AbdElKader et al. [40] incorporating MRR units. Arrows pointing away from the transceiver indicate the transmitted optical signal. Arrows pointing back to the transceiver indicate the retroreflected signal, either with or without RIS.

Finally, a RIS-assisted hybrid RF-UOWC system is compared under NOMA and OMA, using heterodyne detection and IMDD [29]. The relay system includes an RF link from the base station to a surface vehicle via a RIS, and then UOWC connecting to underwater vehicles. They show that at low SNR, the number of elements greatly reduced the outage probability, but the outage probability saturated at high SNR, and the effect of element number was negligible. Power allocation factor is also discussed for the UOWC links, where, while a selective increase for one user could improve system performance, excessive increments could deteriorate it. Overall, NOMA was better than OMA, and heterodyne detection was better than IMDD for SNR greater than 0 dB. The key contributions of these works are summarized in Table 7.

Table 7. A summary of the contributions and benefits from different, novel multiuser strategies proposed for RIS-based UOWCs.

Reference	Key Contributions
Salam et al. [34]	• ASE rises with increasing transmit power across all schemes. • The proposed DMA allocation consistently achieves the highest ASE, followed by EMA, while OMA lags at higher power. • Under ~22 dBm of transmit power (for 6 users), OMA performs the best followed by RSMA, and then OMA. Between ~22 and ~37 dBm, RSMA shows the best SE overall. This is due to better handling of multiuser gain. Beyond ~37 dBm, NOMA outperforms OMA. • ASE improves with more users, especially under the DMA scheme, which scales efficiently. • DMA remains the best performer as the user count grows. • Fairness decreases as users increase, but OMA keeps the highest fairness (since one user per slot). DMA nearly matches OMA in fairness, balancing ASE gains with equitable distribution. • NOMA's fairness drops the most, while RSMA maintains moderate fairness. • ASE is highest under weak turbulence ($\sigma_I^2 = 0.2178$) and low pointing error ($\rho^2 = 6$). DMA is most resilient, retaining higher ASE under adverse conditions. • ASE follows the attenuation levels dependent on the inhomogeneous distribution of optical properties in the water column. This applies to both S1 and S8 waters. However, DMA scheme consistently outperforms EMA, OMA, NOMA, and RSMA at all depths.

Table 7. *Cont.*

Reference	Key Contributions
Naik et al. [37]	• First evaluation of the application of a STAR-RIS for UOWC. • STAR-RIS increased the luminous intensity at the receiver by twofold. • Both transmitted beams and reflected beams are improved. • Analytical results show that STAR-RIS achieves 3.8 $\times$ 10^{-3} BER (FEC rate) at about 5 dB for N = 10 and 9 dB for N = 5, while comparatively the RIS links achieve the same BER at 12 dB for N = 10, and 15 dB at N = 5. These are much better than the LOS link which requires an SNR of about 47 dB. • Incorporating STAR-RIS, HD BPSK showed the best BER performance, followed by HD BFSK, then IMDD OOK and finally 16-QAM. HD BPSK always performs better than 16-QAM by about ~13 dB.
AbdElKader et al. [40]	• Explores the use of RIS and MRRs with advanced modulation techniques like L-QAM-MPPM to enhance UOWC performance. • Derived closed-form expressions for the average BER of L-QAM-MPPM under path loss, Gamma-Gamma turbulence model, and pointing errors, under conventional modulation schemes in clear and coastal ocean environments. • L-QAM-MPPM outperformed conventional modulation techniques in terms of BER and power efficiency, especially under weak turbulence and low pointing error conditions. • Optimal placement of the RIS relative to the transceiver and MRR was critical for maximizing signal quality and efficiency. • L-QAM-MPPM achieved better spectral efficiency than L-QAM and MPPM, highlighting its hybrid advantages in underwater channels.

2.4. Metasurfaces for Underwater Applications

One of the earliest underwater applications of metasurfaces was for polarization imaging. Due to the nature of underwater scattering, light from a target object or source tends to be different from the polarization states of photons available in the background. More about this has been discussed in Section 4.1.2 of this paper. While conventional hardware uses complex manual maneuvering of polarization analyzers, the paper discusses a new design for a polarization-splitting compact metalens-assisted device capable of capturing two orthogonally polarized images [41]. It is made with polycrystalline silicon (poly-Si) nanopillars of rectangular in-plane cross-sections on a 500 µm fused silica substrate. The results demonstrate the improved recovery of blurred images underwater without computationally intensive post-processing, beneficial for real-time imaging by AUVs in turbid environments. The possibility of phase manipulation at a subwavelength spatial resolution with a dielectric metasurface phase mask has also been explored for UOWC [42]. However, the closest work that is adoptable for RIS-application is by Hu et al., where they design a full-color circular autofocusing Airy beam (CAFAB) metasurface [43]. An Airy beam is a form of structured light with mathematically predictable waveforms and distinct propagation characteristics [44,45]. The benefits of such beams for UOWCs are their natural resistance to diffraction, ability to reconstruct itself beyond partial obstructions, and self-accelerating and curved propagation characteristics. In this work, the authors fabricate an ultra-broadband metasurface (440–640 nm) based on basic cells, with 800 nm tall nanopillars of TiO_2 stacked on a SiO_2 substrate with a period of 300 nm [43]. This metasurface converts Gaussian laser beams to Airy beams. Thereafter, the adaptability of the Airy beams is tested experimentally for red, green, and blue (RGB) wavelengths at 637 nm, 517 nm, and 455 nm, respectively, in the presence of obstacles. They are compared against the performance of RGB Gaussian beams. The obstacle size ω_0 was normalized to the maximum transmitter beam aperture (14 mm). The result showed that at 0.43 ω_0, the RGB Airy beams outperformed the Gaussian by a maximum 7.3 Gbps, and that the received optical power (ROP) of red, green, and blue outperformed the Gaussian by approximately

4 dB, 10 dB, and 5 dB, respectively, compared to the Gaussian at 0.57 ω_0. The Airy beams appear particularly resistant to central occlusion, establishing links up to about 1 ω_0 with red, and 0.9 ω_0 with green and blue beams, while the respective maximums for Gaussian were approximately 0.71 ω_0 and 0.57 ω_0, as demonstrated in Figure 5. The Airy beams performed better as well under bubble flow rates of 1 L/min, 6 L/min, and 10 L/min, and bubble areas of 0.89, 1.63, and 2.55 mm^2. Simulated results show that the Airy beams could achieve a data rate of 20.1 Gbps in pure water, and 12.1 Gbps in turbulent water with 0.43 ω_0 occlusion, which is almost double that of Gaussian, at 100 m link distance. The authors further demonstrate the ability to transmit 4K video underwater by transmitting tricolor bitstream, further confirming the superiority of this approach over conventional means. Additionally, Airy beams may be resistant to weak anisotropic ocean turbulence [46]. If this technology is adopted into RIS elements, the dynamic adjustment of the focal points and deflection at the RIS nodes may significantly minimize propagation losses between transmitter and receiver. Finally, a metasurface design is demonstrated which supports direct, high-frequency, bidirectional conversion of microwave signals to optical signals (532 nm) without the need for external power supplies or drives [47]. This is enabled by integrating metal-semiconductor junctions and photoelectric PN junction components into elements with double-sided microwave resonant structures. The conversion efficiencies for input microwave power of 25 mW, and 250 mW are at 10.8% and 6.48%, respectively, due to non-linear intensity-dependent behavior of the Schottky and laser diodes. This may be improved by light-emitting-diodes, which have a higher electro-optical conversion efficiency. The up-conversion switching frequency is demonstrated at 400 kHz, with the down conversion limited to about 100 kHz, mainly due to the high junction-capacitance of the photodiode used for converting received light signals. The authors further demonstrate full-duplex air–water transmissions using OOK, showing that for optical-to-microwave conversions in a turbulent channel, that spatially diverse illuminations of the photodiodes can achieve a more stable outcome being more robust to pointing errors. Such a technology has substantial benefits towards connecting the above-and underwater environments together through less complexity and cost.

Table 8. A summary of the contributions from different works on metasurfaces and/or metalenses that support UOWC.

Reference	Key Contributions
Zhao et al. [41]	• A polarization-splitting compact metalens-assisted device that can capture two orthogonally polarized images simultaneously underwater. • No mechanical movement of optics is necessary.
Ren et al. [42]	• A phase mask to spatially multiplex four green OAM beams through a single aperture. • Two modulation techniques are used: direct modulation (4 Gbps) and IR-modulation with OAM imprinting (40 Gbps), due to a higher modulation frequency ceiling with IR.
Hu et al. [43]	• A full color (440–640 nm) circular autofocusing airy beam meta surface. • Capable of passively converting Gaussian beams to Airy beams.
Wang et al. [46]	• Analytical study of the performance of an Airy beam with power-exponent phase beam carrying OAM in weak anisotropic ocean turbulence.
Zhang et al. [47]	• A meta surface that supports bidirectional, high-frequency conversion of microwaves to optical at 532 nm.

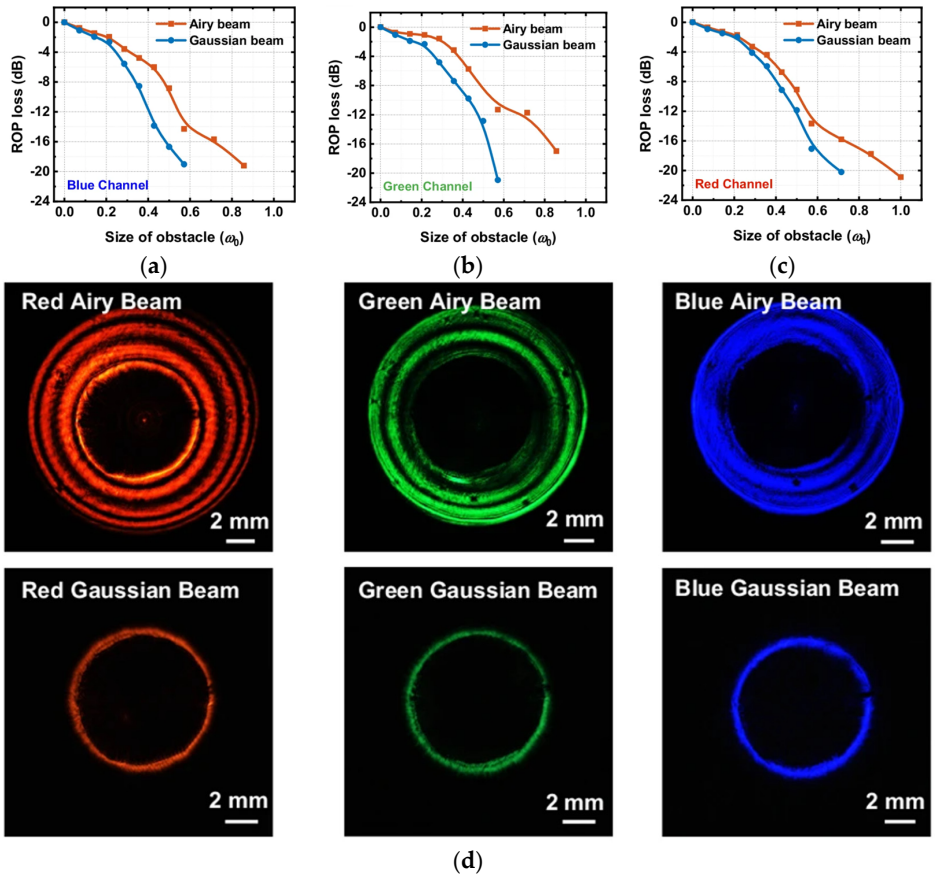

Figure 5. Comparison of loss in ROP between Airy beam and Gaussian beam for different sizes of obstacles in (**a**) red channel (637 nm), (**b**) green channel (517 nm), and (**c**) blue channel (455 nm). The obstacle size is normalized to the beam aperture ω_0 of approximately 14 mm. The images and results are from Hu et al. [43]. In (**d**), the top three are beams received with the metasurface, and the bottom three are the regular Gaussian beams. Table 8 summarizes these works.

3. Acoustic Reconfigurable Intelligent Surfaces (A-RIS) for UWACs

Compared to underwater optical communication, underwater acoustic communication (UWA) has established dominance in complex aquatic environments due to its significantly longer propagation distance and superior adaptability to environmental conditions. While underwater optical communication can achieve higher data transmission rates, its performance is constrained by factors, such as limited propagation range, light scattering, and water turbidity, restricting its applicability to short-range scenarios in clear water environments [2]. In contrast, UWA can reliably propagate over distances of several kilometers in deepwater conditions, offering greater practicality, particularly for long-distance, low-data-rate communication [48].

However, UWA is not without its challenges. Issues, such as limited bandwidth, severe multipath effects, and highly dynamic channel variations, hinder its communication rate and reliability. In recent years, UWA technologies integrated with RISs have garnered significant attention. By intelligently manipulating the propagation paths and directions of acoustic waves, RISs can optimize the signal transmission environment, enhance channel capacity, and improve spectrum efficiency, thereby presenting a novel approach to overcoming the limitations of UWA [49].

Typically, the transmitter and receiver are low-cost devices equipped with single-input single-output (SISO) acoustic transducers. However, in the absence of acoustic RIS, the natural UWA channel suffers from severe multipath effects, resulting in low data rates and unreliable communication.

Acoustic RIS overcomes these limitations by employing beamforming to precisely control the phase and amplitude of incident acoustic waves, thereby creating a strong reflective path with a gain far exceeding that of other natural channel paths. This not only significantly improves the signal-to-noise ratio (SNR) at the receiver but also mitigates the issue of frequency-selective fading. Consequently, the underwater channel capacity and data rates are substantially increased, addressing key bottlenecks in the development of UWA systems.

Compared to traditional UWA, acoustic RIS technology significantly enhances channel gain, suppresses multipath effects, and improves the SNR, spectral efficiency, and data rates by intelligently controlling the reflection paths and phases of acoustic waves. Simultaneously, it reduces bit error rate (BER) and communication energy consumption [50,51]. Moreover, acoustic RIS can achieve comparable performance gains without relying on complex MIMO systems, enabling support for low-cost, low-power underwater devices. This technology exhibits excellent adaptability to dynamic environments and robust capabilities for long-distance communication [52].

3.1. Channel Modeling (A-RIS)

UWA channels exhibit unique propagation characteristics, including multipath effects, time-varying properties, path loss, and low-frequency bandwidth limitations, all of which pose significant challenges to the design and optimization of acoustic RIS systems. Traditional UWA receivers rely on complex adaptive equalizers to compensate for multipath effects in the time or frequency domain, which introduces significant computational overhead and delay. The working mechanism of A-RIS is completely different. It actively creates a strong, dominant LOS or quasi-line-of-sight reflection path by performing beamforming in the spatial domain. This means that the complexity of the equalizer required for the receiver can be greatly reduced, and may even no longer be required under certain conditions, directly alleviating the multipath problem from the root. On the other hand, compared with traditional MIMO, A-RIS unlocks the gain of the spatial dimension in a lower-cost and more energy-efficient way, allowing small, low-cost terminal devices to enjoy the high performance that was previously only achievable with large MIMO systems. Table 9 provides representative quantitative data for a direct comparison of the three schemes in terms of BER, SNR, and energy efficiency. In contrast, while adaptive equalizers and MIMO can effectively combat multipath effects and improve performance, they typically require complex active hardware and high computational processing, resulting in higher energy consumption.

Table 9. Performances comparison between A-RIS, adaptive equalizer, and MIMO strategies.

	BER	**SNR**	**Energy**
A-RIS	Achieves 8 b/s/Hz, with an average BER lower than 10^{-4} [51].	The average received SNR can be improved by 20.8 dB [51].	Operates in passive mode, requiring no power amplifiers or complex signal processing units. Power consumption is very low [51].
Adaptive Equalizer	Spectral efficiency of 0.4 b/s/Hz, where the BER decreases from 9.2% to 1.6% [53].	Experiments show that the output SNR can be increased by 0.4–1.8 dB [54].	Higher power consumption, since complex signal processing is required.
MIMO	Spectral efficiency of 1.76 b/s/Hz, achieving zero BER [55].	Compared with single-link systems, MIMO achieves a diversity gain of more than 5.2 dB [56]	Higher power consumption, as multiple transmitters and complex signal processing are needed.

As shown in Figure 6, Ray propagation theory and wave theory are the primary methodologies employed for RIS-assisted UWA channel modeling. Commonly used modeling tools include BELLHOP, COMSOL, and VirTEX. To address the unique channel characteristics of UWA communication, Edemen et al. [52] constructed a channel impulse response (CIR) model for acoustic RIS communication systems. The VirTEX toolbox was utilized for channel modeling, with a particular focus on evaluating the potential of RIS in enhancing the performance of UWA systems. Recognizing the physical properties of acoustic wave propagation, Sun et al. [50] proposed a hybrid modeling approach that integrates COMSOL Multiphysics simulation with BELLHOP ray-tracing to establish an acoustic channel model. This model is employed to simulate and predict the propagation paths, shadow zones, and convergence zones of acoustic waves in complex underwater environments. Similarly, Kisseleff et al. [1] utilized the COMSOL Multiphysics simulation platform to evaluate the performance of multilayer reflectors under varying load conditions. To enable active acoustic RIS coverage of underwater shadow zones and achieve seamless communication, Zhao et al. [57] focused on channel modeling for UWA shadow zones. Shadow zones are typically located below this waveguide layer, and the coverage and shadow zone boundaries are defined through formulaic descriptions.

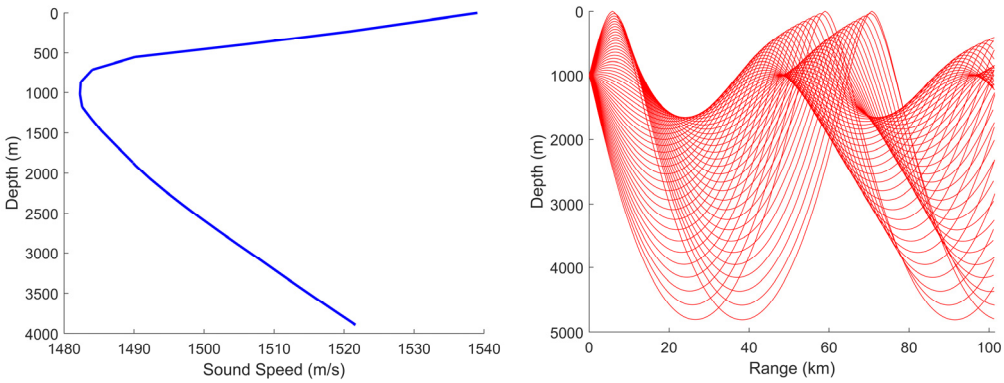

(**a**) (**b**)

Figure 6. Underwater acoustic channel based on ray propagation. (**a**) Sound speed profile. (**b**) Propagation loss of underwater acoustic channel.

3.2. Multiuser Communication and Protocol

As an emerging technology, RIS offers the potential to optimize communication performance in complex UWA environments through dynamic control of acoustic wave reflections. To simplify system deployment, Sun et al. [50] proposed an acoustic RIS-assisted underwater 3D network architecture, which supports coverage of large 3D spaces. A lightweight RIS operation protocol was developed that does not require modifications to the communication protocols of terminal devices.

Dong et al. [58] introduced a novel data transmission and resource allocation method specifically designed to address the energy hole problem in UWA networks. Through data classification, RIS partition optimization, and genetic algorithms, this method significantly enhances data transmission efficiency and network performance, providing critical technical support for the sustainable operation and efficient management of UWA communication networks.

3.3. Wideband Beamforming

To address the wideband characteristics of UWA communication, Sun et al. [50] proposed a wideband beamforming scheme capable of effectively mitigating signal dispersion. By carefully designing the circuit parameters of piezoelectric reflectors, the internal disper-

sion within a single reflection unit and the dispersion between units are counterbalanced, aligning the wavefronts of reflected signals of different frequencies in the same direction. This approach overcomes the beam misalignment challenges of wideband signals, which creates a huge security capacity advantage and provides a key performance benchmark and feasibility proof for subsequent research on how A-RIS can suppress eavesdroppers through beamforming. Wang et al. [51] developed a practical wideband beamforming algorithm by maximizing the normalized power summation of signals at different frequencies in the target direction, thereby achieving effective wideband beamforming. Luo et al. [59] introduced IQ modulation, which enables reflected waves to have arbitrary amplitude and phase control, supporting precise beam steering. Compared to traditional 1-bit or 2-bit coding schemes, IQ modulation provides greater flexibility, reduces sidelobe interference, and optimizes beam direction. The performance of acoustic RIS was evaluated through tank and lake experiments.

3.4. Hardware Designs

Unlike electromagnetic waves, sound waves require mechanical reconfigurability to achieve effective reflection, whereas the metallic patch reflectors used in terrestrial RIS cannot manipulate the mechanical properties of sound waves. To address this issue, acoustic RIS incorporates the piezoelectric effect. Piezoelectric transducers, commonly used in UWA communication, are employed as reflection units. These transducers are arranged into arrays to form the acoustic RIS. By adjusting the circuit branches of the transducers, the piezoelectric effect can control the vibration of the piston surface, enabling reconfigurability and precise control over the phase of the reflected sound waves.

Each reflection unit in the array is independently connected to a controller, enabling high-resolution beamforming. Sun et al. [50] proposed an acoustic RIS hardware design based on a piezoelectric reflection array, where each reflection unit adjusts the reflection phase via the piezoelectric effect. Microcontrollers are used to elastically control the reflectors in real time, achieving precise sound wave reflection and phase tuning. The design proposed by Wang et al. [51] utilizes piezoelectric reflection units with the same structure as the Tonpilz transducers widely used in existing UWA communication systems. These Tonpilz transducers are connected to controllers, and the reflection of sound waves is manipulated by adjusting their impedance. Using their inherent piezoelectric effect, these units directly reflect incident sound waves without requiring signal reception, processing, or retransmission modules. This approach simplifies the system architecture while maintaining efficiency and adaptability in underwater environments. For the design of multilayer acoustic reflectors, Kisseleff et al. [1] proposed that each acoustic reflector is composed of multiple piezoelectric ceramic (PZT) discs arranged in a Tonpilz structure. The head mass facilitates effective vibration, while the central PZT stack adjusts the phase and amplitude of the reflected waves through independently controlled load impedance. Using an "acoustic coupling" mechanism, each layer of PZT can operate independently, enabling flexible regulation of the reflected signals. Simulation results demonstrate that even in dynamic ocean environments, the multilayer acoustic RIS (ML-ARIS) can maintain stable reflection performance.

To address the dual challenges of communication enhancement and location privacy protection in shallow water environments, Chen et al. [60] proposed an acoustic RIS architecture integrated with an artificial noise (AN) module. By jointly optimizing transmission beamforming, reflection precoding, and noise factors, the architecture maximizes communication performance while safeguarding location privacy. Similarly, with 24 Tonpilz-structured reflection units, Liao et al. [49] optimized acoustic impedance matching between water and sound for each reflection unit. Using ultra-low-power microcontrollers and

programmable load networks, the amplitude and phase of the reflection units can be precisely controlled. Luo et al. [61] utilized microcontrollers (MCUs) to dynamically control load impedance, combined with I/O expanders for efficient management of the unit array. The system supports three operational modes: phase adjustment, passive reflection, and deep sleep. With low power consumption, the system is powered by ocean energy harvesting devices.

A full summary of the research works and contributions on acoustic RIS are provided in Table 10.

Table 10. A summary of contributions in acoustic-RIS.

Reference	Key Issue	Solution	Performance
Sun et al. [50]	Incompatibility between high data rate and long range in underwater acoustic communications.	Novel acoustic RIS hardware using piezoelectric reflector arrays and operation protocols.	Channel Capacity: P2P data rate increased from <2 kbps to hundreds of kbps (two orders of magnitude).Coverage: Achieved communication ranges of several kilometers.Energy Efficiency: Total power consumption for an active 60 × 60 RIS is 90 mW.System Complexity: Lightweight protocol requiring no changes to end-user devices.
Wang et al. [51]	Low data rate and high cost of MIMO in UWA communications.	Active piezoelectric RIS hardware and hybrid wide-narrowband beamforming.	Channel Capacity: System capacity increased by up to 8.2 bps/Hz.Energy Efficiency: Total power consumption reduced by over 95% to achieve the same modulation (QAM256).System Complexity: Lightweight non-intrusive protocol requiring no modifications to end devices.
Edemen et al. [52]	Channel fading and multipath limit UWAC transmission efficiency.	Model RIS-assisted UWAC channel and analyze CIR under different RIS configurations.	RIS maintains underwater acoustic channel sparseness.
Zhao et al. [57]	Shadow zones cause discontinuous underwater network coverage.	Deploy acoustic RIS at sound channel axis (deep sea) and seabed (shallow sea) to actively control acoustic reflection for enhanced coverage.	Coverage: <20% without RIS, nearly 100% with optimal RIS deployment. System Complexity: 10 RIS units for 10 km shallow sea coverage; 20 units for non-optimal placement. Propagation Delay: 99% phase deviation reduction after correction for 50 cm vertical displacement. Energy Efficiency: RIS array size N = 20 maintains stable performance across deployment depths.
Dong et al. [58]	Energy holes cause data transmission interruption and accumulation in UWAN.	Use AUV equipped with RIS for classified data forwarding, optimize RIS chunking scheme based on data importance using genetic algorithm.	Transmission Time: 59% reduction compared to AUV-only (non-RIS) scheme. Transmission Efficiency: Simultaneous reflection to multiple destination nodes. System Complexity: 30 × 30 RIS array implementation Energy Efficiency: Enhanced through data importance classification and RIS chunking optimization.
Chen et al. [60]	Location privacy vulnerable to eavesdropping nodes in underwater acoustic communication.	Design RIS system with artificial noise module, jointly optimize transmit beamforming, reflective precoding and noise factor for enhanced communication, and privacy protection.	Location Error: 14.5× increase compared to conventional RIS. Coverage: 97% improvement over non-RIS system. System Complexity: 512 reflection elements RIS array.

Table 10. *Cont.*

Reference	Key Issue	Solution	Performance
Luo et al. [61]	Address incompatibility between acoustic wave physics and existing RF-RIS designs.	Design 1-bit phase coding UA-RIS based on load network with 24 reflection units for passive acoustic beamforming.	Propagation Delay: 20 ms phase switching period at 21 m communication range. System Complexity: 6 × 4 array with dual-PZT reflection units. Energy Efficiency: Phase manipulation requires only several mW, suitable for energy harvesting.
Liao et al. [49]	High transmission power and strong interference.	Jointly optimizing acoustic RIS reflection angle and signal frequency to minimize total transmission power.	Channel Capacity: Channel capacity is improved through optimization, with specific values dependent on transmission distance and frequency.Energy Efficiency: The lowest interference reaches −30 dB at the optimal reflection angle (0°) and frequency (4×10^5 Hz), indicating significant energy efficiency improvement.

Furthermore, a brief overview comparing the key features of O-RIS and A-RIS are provided in Table 11.

Table 11. A brief comparison and overview of O-RIS and A-RIS.

	O-RIS	A-RIS
Operating Principles	Manipulates the electromagnetic properties (e.g., refractive index, permittivity) of RIS elements to alter the phase, amplitude, and polarization of incident light waves, thereby reshaping the optical field.	Manipulates the mechanical vibration characteristics (via the piezoelectric effect) of RIS elements to alter the reflection phase of incident sound waves, achieving acoustic field focusing and beamforming.
Physical Medium	Electromagnetic Waves	Mechanical waves.
Hardware Implementation	Mirror-arrays, metasurfaces	Piezoelectric transducer arrays.
Key Advantages	Extremely high bandwidth, very high data rates, low latency, immunity to electromagnetic interference.	Long propagation distance, strong non-line-of-sight capability, technology is relatively mature.
Challenges	1. Short Propagation Distance 2. Line-of-Sight Dependency 3. Ambient Light Noise 4. Turbulence Effects	1. Limited Bandwidth 2. Multipath Effects 3. Wideband Beam Squint 4. Dynamic Channel
Channel Modeling	Focuses on absorption/scattering coefficients (related to Chl-a, CDOM, etc.), turbulence models, and pointing errors.	Focuses on ray tracing, multipath delay spread, sound speed profiles, and the formation and coverage of acoustic shadow zones.
Research Directions	Hybrid FSO/RF-UOWC networks, physical layer security, NOMA/RSMA for multiuser access, STAR-RIS, metasurface-based higher-order beam generation, and signal conversion.	Hardware design and integration, wideband beamforming algorithms, lightweight communication protocols, shadow zone coverage, and network energy efficiency.
Applications	High-speed underwater data center interconnects, high-rate data offloading from AUVs to base stations, real-time high-definition video streaming, secure short-range communications.	Remote data collection from underwater sensor networks, cross-basin communication, underwater navigation and positioning, long-term low-power communication with surface vessels.

4. Research Challenges

The survey conducted highlighted that the current state-of-the art in underwater RIS was mainly focused on the physical layer aspects. This is mainly due to the underwater environment being a more drastic and dynamic channel that terrestrial channels with unique, time-varying channel conditions which researchers have not been able to fully grasp yet. Here, we have attempted to discuss in-depth some key and often overlooked unique channel conditions and challenges, incorporating the latest research and use it to highlight potential opportunities.

4.1. Environmental Challenges

4.1.1. Effect of Varying IOPs in Stratified Oceans

Light transmissions underwater experience loss due to absorption and scattering. The linear sum of these coefficients produces the beam attenuation coefficient, $c(\lambda)$. Thus, the light intensity I_t at a distance, d, can be evaluated using the Beer–lambert Law, given as $I_t = I_0 e^{-c(\lambda)d}$, where I_0 is the initial transmitted irradiance.

The absorption is primarily dependent on the absorption by water molecules, colored dissolved organic matter (CDOM, usually chemical releases from decaying matter), phytoplankton (green algae), and detritus (organic and inorganic debris). The scattering relates to photons directed away from the intended path due to incidence mainly with particles, such as the water molecules, phytoplankton, and detritus. All water bodies have different compositions of each, and thus the inherent optical properties (IOPs) at each location will be different. However, commonly categorized as clear open ocean, coastal oceans, and turbid harbors, ocean types can be further categorized by the ten Jerlov Types I-III (clear, open oceans) and 1C-9C. The spectral response of light to each of these constituents is unique and has been thoroughly studied. Shorter wavelengths in the blue-green spectrum are preferred in clear open oceans while the yellow-amber spectrum may be better in coastal water. The attenuation coefficients in Jerlov waters are widely adopted in UOWC analyses.

However, Jerlov classifications assume a water column is homogeneous, whereas in the real world, ocean columns are more commonly stratified (in layers). This is a result of both ocean dynamics and external factors such as the nature of wind and sunlight. It can be identified with conductivity, temperature and depth (CTD) measurements, and be observable even within depths of a few meters up to several kilometers. Given a LOS UOWC has an upper-limit range of a few hundred meters in the clearest waters, UOWCs need to be designed with the awareness of stratification in mind.

For example, the immediate water layer beneath the sea surface shows a consistent, mixed characteristic, marked by constant temperature, salinity, and Chl-a levels. This is the surface layer. Thereafter, a steep decline in salinity and temperature (thermo- and halocline) marks the transition to a mid-water region. In here, due to the abundant presence of sunlight closer to the surface, and depleting level of nutrients further up, a relative-Gaussian depth-profile of the Chl-a present organisms can be found. Chl-a is a primary constituent of chlorophyll and strongly signifies the presence of algae. Along this depth is a point at which with optimal sunlight and nutrient availability, Chl-a reaches a maximum concentration, which is called the deep-chlorophyll maximum (DCM). Locations closer to the shore are often higher in Chl-a due to higher nutrient availability than open oceans. Stratified waters, however, can be categorized into nine types, S1-S9 by their Chl-a profile, in order of increasing turbidity [35]. The depth-profiles can be derived using Equations (1)–(3) [62], and coefficients in Table 12 in [36]. Here, z, is the vertical depth; the standard deviation, σ, of the Gaussian profile is defined in (2) [36,62]; B_0 is the background Chl-a concentration at sea-surface; s is the vertical gradient of decline of Chl-a concentration; h is the total Chl-a concentration above the background value; z_{max} is the depth at which DCM

occurs and C_{max} is the Chl-a concentration at this depth. The depth (z_∞) at which Chl-a concentration approaches near zero is determined by (3) (a theoretical limit). Approaching the seafloor, there is usually another distinct halocline where salinity increases marking the transition to bottom water. The depth profiles are visualized in Figure 7.

$$C_c(z) = B_0 + (s \times z) + \left(\frac{h}{\sigma\sqrt{2\pi}}\right) e^{\left(-\frac{(z-z_{max})^2}{2\sigma^2}\right)} \quad (1)$$

$$\sigma = \frac{h}{\sqrt{2\pi}(C_{max} - B_0 - s \times z_{max})} \quad (2)$$

$$z_\infty = \frac{-B_0}{s} \quad (3)$$

Table 12. Parameterized coefficients for vertical Chl-a concentration distribution [36].

Type	B_0 (mg m^{-3})	$s(\times 10^{-3})$ (mg m^{-2})	h (mg m^{-2})	C_{max} (mg m^{-3})	z_{max} (m)	z_∞ (m)
S1	0.0429	−0.103	11.86	0.174	114.6	415.5
S2	0.0805	−0.261	13.86	0.237	90.6	309.5
S3	0.0801	−0.284	18.54	0.244	79.9	282.2
S4	0.144	−0.544	15.42	0.300	62.2	264.2
S5	0.211	−1.05	14.37	0.389	43.3	200.7
S6	0.160	−0.706	21.24	0.460	31	226.8
S7	0.332	−1.96	20.06	0.637	20	169.1
S8	1.014	−9.09	17.48	1.31	13.9	111.5
S9	0.555	0	90.02	3.17	9.9	–

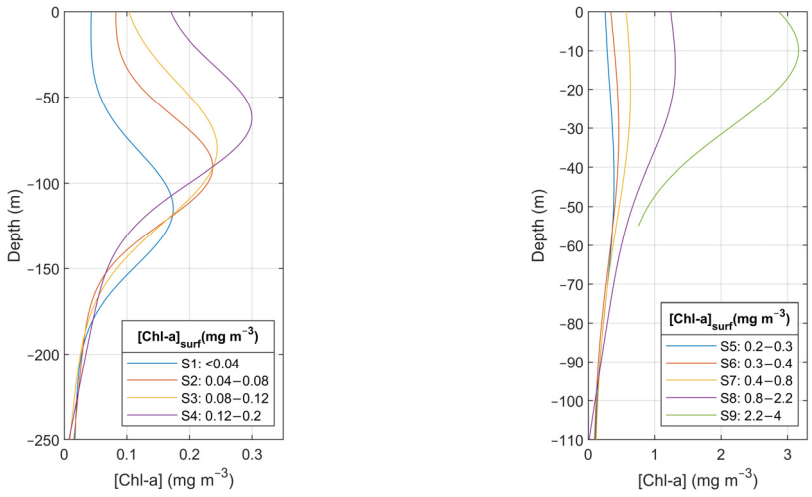

(**a**) (**b**)

Figure 7. Reconstructed vertical Chl-a concentration profiles for S1–S9 [36]. The clear ocean profiles are shown in (**a**), and the coastal profiles are shown in (**b**).

The IOP profile along the depth can be derived using Haltrin's single parameter model, based on the Chl-a concentration [14,63]. These can be adapted as Waduge et al. for UOWCs, which shows that for diffused-line-of-sight and point-to-point links, the attenuation at the DCM causes a significant loss in optical-SNR (OSNR). The results show a low attenuation region above the DCM in S1–S4, which worsens towards S8; and a low attenuation region below the DCM whose depth gradually shifts upwards with increasing profile turbidity. This implies that perhaps it is better to reach the destination through a low-attenuation NLOS path if closer to the DCM. This effect is more pronounced in clear open oceans and

shows a preference for green to amber wavelengths (~500-570 nm) at the DCMs of S1 to S8, respectively, and blue wavelengths (~430 nm) in the low attenuation regions, in the absence of sunlight. It is also observed that generally for short links, a longer wavelength is preferred overall, dependent on the spectral responsivity of the photodiode.

4.1.2. Solar Interference

The level of radiance reaching the sea surface changes throughout the day as well as seasons. The spectrum can be further impacted by cloud cover. The Sun's azimuth and zenith angle at the location of interest changes due to the Earth's rotation, axial tilt, and elliptical orbit around the Sun, causing the penetrating light rays to be refracted at an angle at the air–water boundary. Due to the diffusive nature of the ocean water, although there is a significant difference between downwelling and upwelling sunlight, it gradually evens out to an indistinguishable value further deep [64]. Here, a receiver, even if pointed vertically down, will not be fully immune to it. Accurate site-specific downwelling spectral distribution is best obtained through in situ measurements, which can be resource intensive. Alternatively, sunlight models, such as SPCTRL2 [65], SMARTS2 [66,67], or MODTRAN [68], may be a good alternatives to estimate the spectra based on date, time and location (latitude and longitude), and atmospheric data available. Generally, the blue-green spectrum is at the highest intensity, as seen in Figure 8. This also corresponds to the spectrum with the most penetrative ability underwater [69]. Due to this, OSNR analysis especially in stratified, clear, open oceans show that although the blue-green spectrum is usually preferred, a longer wavelength spectrum would provide relatively higher OSNR at short-range within the euphotic zone (depth at which sunlight reaches 1% of sea surface) [70].

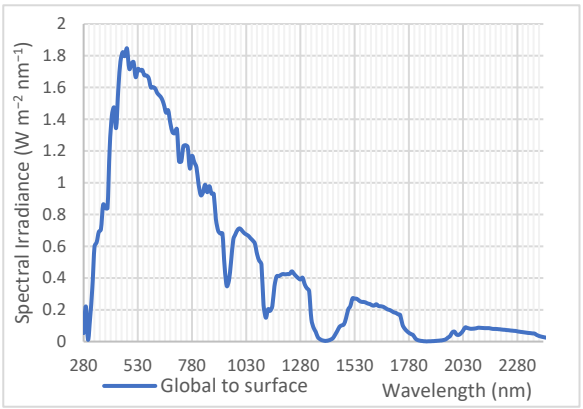

Figure 8. Spectral distribution of global irradiance generated for a clear summer day in Auckland, New Zealand, by SPCTRL2 for the 7 December 2023 at 11:30 am; coordinates, 36.8509 S, 174.7645 E; 2.2 cm precipitable water vapor, 1013 mb atmospheric pressure, and 300 DU ozone coverage [70].

Usually, this depth-spectral behavior has been studied for homogeneous Jerlov types, which has recently been extended by Waduge et al. for stratified columns [36]. Some parameter depth-profiles are available in Figure 9, collected by us from a coastal location during a voyage into the Hauraki Gulf, New Zealand. Some inter-dependent relationships are also visible here.

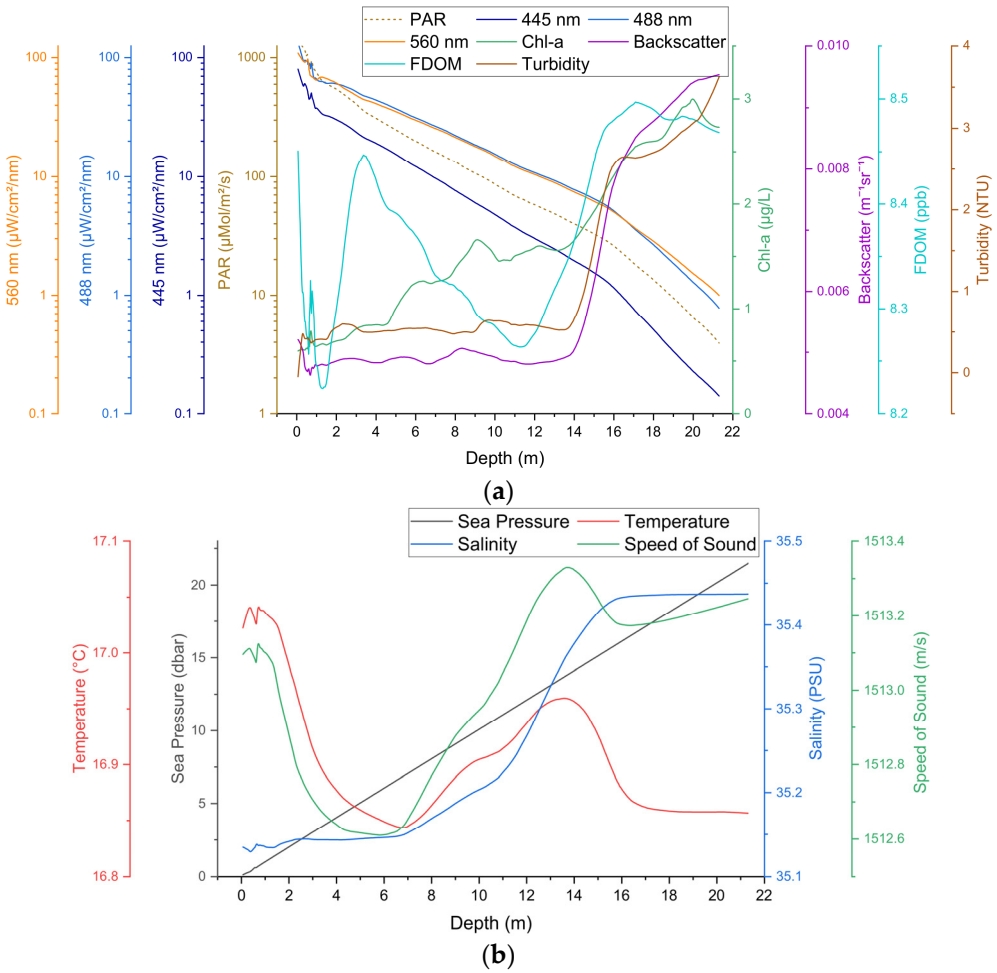

Figure 9. (**a**,**b**) Shows the inhomogeneous depth-dependent distribution of various underwater parameters that may influence optical and acoustic UWCs at a single coastal location off the coast of the Hauraki Gulf, New Zealand.

Furthermore, light reaching the Earth from the Sun, Moon, and other stellar bodies are mostly parallel and unpolarized (having randomized electric field vectors or e-vectors). When such beams travel through various media that introduce differential scattering, differential absorption, or differential reflection, such as a dielectric medium, the beam at the point of observation tends to often be partially linearly polarized (plane-polarized). Given that water is a strong dielectric, the light reflected off the surface, refracted into the water body, and scattered within will show high plane polarization [71]. The level of polarization of solar irradiance is directly related to the Sun's zenith angle and more prominent within the Snell's window underwater (Figure 10 shows an illustration and Figure 11 shows Snell window at different depths in the Black Sea).

Realistic expressions of underwater polarization of downwelling sunlight have been modeled to be the cumulative outcomes of Mie and Rayleigh scattering, and suggests it will lose its polarization characteristics with distance [72,73]. This ambient light is often predominantly horizontally polarized, while stray reflections from fish and reefs may have distinct polarization patterns based on the organism's adaptations [74]. This phenomenon has been utilized for underwater image restoration; popularly for "de-hazing" as explained by Raihan et al. [75]. Mullen et al. [76] notes that effective polarization-discrimination would need to isolate the polarization influences of first, the medium, and then of the target. In their work, Mullen et al. [76] have investigated utilizing polarization discrimination to suppress backscattering in an retroreflector based UOWC link, building upon findings from

Vasilkov et al. [77] that showed polarization levels at 85–90% in clear waters and at relatively lower 70–80% in turbid waters within depths of 28–33 m that correspond to the euphotic zone. This coincides with the depths at which IOPs experience much variability in stratified oceans, and thus polarization characteristics may also show a depth-spectral-profile, which to the authors' knowledge, has not yet been investigated.

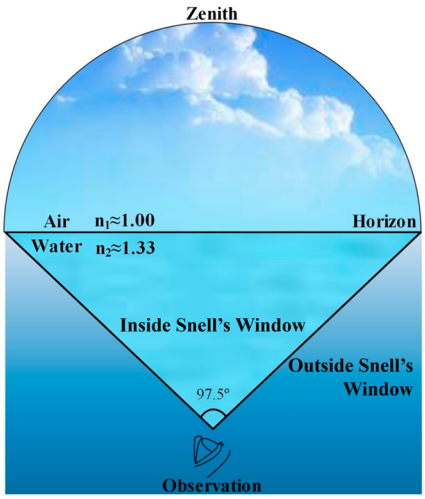

Figure 10. Snell's window—a circular 'window' of light caused by the refraction of direct and scattered sunlight upon incidence with the water surface [78].

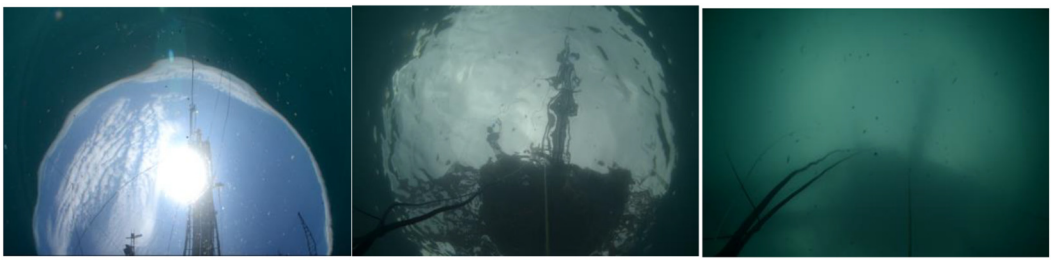

(**a**) (**b**) (**c**)

Figure 11. Photographs of Snell's window in the Black Sea for (**a**) for a flat sea surface at depth 0.5 m, (**b**) for a rough sea surface at depth 1.5 m and (**c**) 5 m. (The attenuation coefficient estimated about 0.6 m^{-1}) [79].

In addition, backscattered light from a polarized light beam often retains its degree of polarization, than that scattered by an object, but a more specular target object depolarizes the reflected light less [76]. However, circularly polarized light is more easily depolarized upon incidence with a target object than linearly polarized [80], but is more resistant to depolarization effects from propagation within the medium [81].

However, although polarized UOWCs have been studied broadly, and polarization of ambient light utilized in underwater image processing, utilizing these effects to mitigate ambient light and improve SNR have not been explored.

4.1.3. Light Scintillation Due to Turbulence

Oceanic environments are characterized by turbulence, which is when fluids mix in a disorderly manner. It depends on the length of the fluid, the velocity and its kinematic (eddy) viscosity [82]. Flows characterized by Reynold's number $Re > 2700$ are considered turbulent. In the ocean, the largest eddies could be several kilometers wide (called the outer scale, where length scale is comparable to whole flow), slowly eroding away their energy and diminishing in size reaching the Kolmogorov microscale (inner scale), at

which point, the viscous forces cause the energy to be dissipated as heat and the eddy disappears. Turbulence introduces scintillations in optical transmission, described as the intensity fluctuations in the received signal, which underwater, is dependent on the varying salinity and temperature levels. Several power-spectra, such as the Hill spectrum, Nishikov and Nishikov spectrum, Li spectrum, and quite widely, the Oceanic Turbulence Optical Power Spectrum (OTOPS) model, are used, with which the scintillation index is derived [83]. Turbulence-induced fading has been modeled by the log-normal distribution for weak turbulence characterized by scintillation indices less than 1, and Gamma-Gamma distribution and exponential-Weibull distribution across all turbulence regimes supported with experimental results. A unified turbulence channel model is proposed by Zedini et al. that incorporates effect of bubbles, with good fit with Weibull and exponential-Gamma distributions [22]. Turbulence and signal propagation characteristics underwater have been extensively studied, and we refer the reader to Baykal et al. [83]. For such cases, metasurface-based beam conversion may be highly useful, as discussed under Section 5.

4.1.4. Influences of Time-Varying Effects on the UWA Channel

The time-varying challenges of UWA channels arise from the deep coupling between their physical propagation mechanisms and the dynamic nature of the marine environment. Based on the ray-tracing model, the spatiotemporal variations in temperature (T), salinity (S), and depth (D) directly alter the sound speed profile (c) [84]. According to empirical formulas, these fluctuations induce dynamic changes in the curvature of acoustic rays and the propagation delay.

$$c = 1448.96 + 4.591T - 0.05304T^2 + 1.340(S - 35) + 0.0163D \quad (4)$$

The Pierson–Moskowitz spectrum model for rough sea surfaces and the non-stationary scattering caused by seabed sand waves (generalized WSSUS model) further contribute to the stochastic disruption of propagation paths [85,86]. Additionally, the mobility of communication nodes introduces time-varying phase distortion through Doppler shift effects [87]. Environmental disturbances, such as turbulence vortices and spectrum internal waves, induce phase modulation and energy fluctuations in acoustic wave propagation [88]. The multipath delay spread, comparable to the symbol duration, significantly amplifies inter-symbol interference, as can be seen in Figure 12.

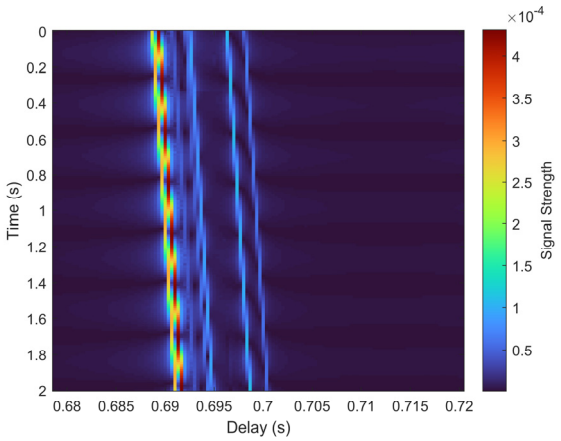

Figure 12. The time varying channel impulse response. The colorbar shows the normalized signal strength.

Compared to optical communication, the inherently low propagation speed of acoustic waves exacerbates the time-varying effects of these factors, posing a critical challenge for real-time channel adaptation in underwater acoustic RIS systems.

4.2. System Challenges

4.2.1. Secrecy and Security with O-RIS

The survey on the uses of O-RIS in improving security discussed in Section 2.2, highlighted that the ASC and SOP is mainly dependent on the channel conditions, particularly, the spectrum-dependent attenuation level and turbulence strength (based on salinity and temperature gradients, and bubble levels). In the previous sections, we discussed how the dynamic underwater channel, even at a given location, could vary across the vertical column. This opens significant opportunities for further investigation, with implications probably unique to the water type, location, and depth. For example, the nature of salinity distribution in the vertical column is generally different between low latitude oceans compared to high latitude ones, with salinity of the surface water especially dependent on evaporation, precipitation, and dilution by river inputs or glaciers melts [89]. This is also the case for temperature and water density. Through this, coupled with the nutrient and sunlight availability of the location, one could achieve a unique set of condition permutations which they could utilize to improve system security with. For example, schemes could be devised to utilize these inhomogeneities to enhance the BER at the eavesdropper compared to the receiver, minimize directional leakages, or intentionally increase BER of the exposed side-channels; utilize wavelength-selective schemes (taking advantage of the depth-spectral distribution of attenuation in stratified waters [36]) for more robust links under sunlight noise and/or artificial jamming.

4.2.2. Multiuser Strategies with O-RIS

Similar shortcomings in modeling the dynamic underwater channel in secrecy and security analyses from an IOP, sunlight and turbulence perspective should also apply to determining optimal multiple access strategies. This would be essential for optimizing resource allocations and user fairness, especially in the power domain schemes for NOMA. For example, in a stratified column, assuming a mobile link is established in the high-attenuation region of the DCM, it would assign a 'low power' to the near user and a 'high power' to the far user. However, if the same assignment levels are used when the user has moved below the DCM, where the attenuation is drastically reduced, such as in S7 and S8 waters, there may be potential that the 'low power' signal would travel all through to the far user possibly causing interference instead either directly or through multipath effects, or by power saturation. The same is true for vertical links with an added caveat of sunlight, which could significantly affect the uplinks. For example, the transmitter below would have to account for the level of sunlight the far user, positioned above, experiences to maintain adequate SNR, in an uplink where the far user is within the euphotic zone, which is also where the DCM occurs. These ambient light effects would only worsen should the far user be closer to the surface. In such a case, perhaps even wavelength-division-multiplexing (WDM)-based OMA systems may be more appropriate as suggested by Waduge et al. [36]. Allocating much higher transmission power may not be feasible for battery-operated systems. Instead, perhaps shifting to a frequency domain NOMA with successive interference cancellation, where a smaller switching frequency is allocated for the far signal may be an option [90]. Given the effect of sunlight polarization discussed previously, polarization–division–multiplexing (PDM) based schemes may have possible advantages, which have not yet been researched in this context. Active manipulation of polarization should be easily achievable through liquid crystals, and more recently, optical

metasurfaces [4]. However, it is evident that all such strategies would need to accurately perform channel state information (CSI) estimations. There are several research gaps in this area.

5. Research Opportunities

5.1. Towards Overcoming Channel Condition Effects on UOWCs

In oceans that are stratified by IOPs, the use of non-linear photonic metasurfaces could be a fantastic use case to convert light of a particular wavelength traveling from a low attenuation region to a high attenuation one [91]. For example, the state-of-the-art in non-linear photonics has demonstrated the ability to perform frequency conversion of light using dielectric metastructures [92]. The demonstration by Gao et al. is one such example where subwavelength-thick nanostructures are shown to convert infrared wavelengths to ultraviolet, with very little absorption by the substrate [93]. Furthermore, conventional RIS could be another solution, by capitalizing on its ability to reflect at any angle and thus, reach the destination through a least attenuated path. However, strategies need to be re-thought to optimize for spectral dependencies. For example, DMA, explored in Salam et al. [34], would also need to consider the depth location of the destination. If the transmit wavelength, experiencing low attenuation at initial location, needs to reach a high-attenuation destination, it would require a higher number of element allocation, potentially with active beam-steering to minimize geometric spreading losses. Such underwater properties further imply that secrecy and security schemes for RIS could be further improved using clustering and screening strategies (like in Tian and Zheng [33]) based on the optimal wavelength for that particular link [36], even forming localized macro and micro cells, such that eavesdropping could also be mitigated. For example, using short-wavelength transmissions for RIS clusters below the DCM during daytime and longer wavelengths in clusters within the region of the Chl-a peak, could naturally introduce robustness towards eavesdropping from the opposite locations, because short wavelengths are significantly attenuated in the presence of phytoplankton in the DCM and also overtaken by the strong blue-green spectrum of sunlight, while the longer wavelength transmission at the DCM, which is more resistant to sunlight, will travel short distances beneath the DCM due to high absorption in water [36].

For mitigating ambient light, an easy approach could be to transmit through a NLOS path beneath the source and destination. This way, the receiver would be pointed below the horizontal, in which case the sunlight interference would be much less. However, a more effective approach could be polarization-based discrimination. This may be beneficial to contrast UOWCs within the euphotic zone for SNR. For example, in clear waters, it may be better to use vertically or circularly polarized UOWCs while discriminating against the horizontally polarized ambient light at locations closer to the sea surface. Further deep, plane-polarized UOWCs could be used, benefitting from its overall depolarization resistance. For such a case, perhaps a RIS node employing gap-plasmon metasurface elements, such as by Ding et al. [94], could be adopted, which simultaneously causes anomalous reflection of the y-polarization portion of incident light at 30.6°–37.9°, while the x-polarization results in surface plasmon polariton (SPP) excitations. The polarization angle is with reference to the phase gradient direction of the metasurface elements. The SPPs excited from the ambient light could simultaneously be converted to energy that powers the RIS, or used to amplify the signal by integrating with technologies as used in solar-cells [95]. It may be further possible to deflect and separate the x- and y- polarization at two different angles using multifunctional metalenses [96,97]. Such RIS-aided polarization-selective techniques may also prove beneficial for improving system security.

Incorporating many such additional dimensions (polarization selection, spatial multiplexing, introducing artificial channel randomness, and intuitive clustering schemes, etc.) with O-RIS for UOWCs may enhance the channel's entropy, while maintaining high channel reciprocity between the sender and the receiver (necessary for well-designed secure key distribution and encryption). For example, to actively distort the eavesdropper's channel, RIS elements could reflect artificial optical noise (from sunlight and background illuminants) towards the unintended listeners while simultaneously maintaining the intended one at high SNR. However, for such schemes, it may be beneficial for the RIS to be an active participant in the key-distribution (and/or encryption) protocol. There is significant research potential in future works for working out how this may be realized.

RIS that combines all such strategies discussed previously, could separate the vertically polarized signal from the horizontally polarized ambient light (Zhao et al. [41], Ding et al. [94]) and convert the full received ambient spectrum to the narrow bandwidth transmission signal. This could be activated by an incoming low power UOWC signal. This way a downlink signal could always be ensured to have high SNR, as the full incident solar spectrum on a large area (based on RIS surface) is converted to one transmission. When there is atmospheric shading (clouds, boats, etc.), the signal amplification will be less, but ambient light will also be low; but the converse would be true when it is sunny. Perhaps the uplink could utilize Fraunhofer bandgaps (spectrum gap in sunlight) [98]. However, such realizations need to be tailored to underwater environments, designing the refractive indices and dielectric properties of the meta-elements with consideration of the vertical salinity and temperature gradients underwater that can alter the permittivity and conductivity along a water column. This is especially true for stratified bodies that exhibit distinct halo- and thermoclines. For example, it has been shown that polarized beams, and higher order beams, such as Orbital Angular Momentum, Bessel and Bessel-Gaussian beams, etc., may be less effected by turbulence [42,83,99–101]. These may be effective at overcoming turbulent effects not only caused by temperature, salinity gradients, and bubbles but also those created by movement of aquatic creatures. However, they each have pros and cons in application, from simplicity, diffraction, self-healing, and energy efficiency perspectives. Therefore, RIS may be ideal for converting one beam-type to another based on what is advantageous for that link environment. This could be performed using works such as Hu et al. [43] and Ran et al. [42]. Thus, the research potential of this field is significant. It may be worthwhile exploring such strategies with the help of artificial intelligence (AI).

5.2. O-RIS with Higher-Order Beams for Mobile Applications

For mobile UOWCs, generally wide-beam emitters, such as LEDs, are often preferred due to accommodating wider coverage and simplifying pointing requirements [99,102]. However, unlike terrestrial FSO, the high, negative-exponential path loss from absorption and scattering often is a prominent loss factor, in addition to loss by spatial geometric spreading of the optical energy [103]. In addition to this, LEDs are inherent with hardware limitations, in that the modulation bandwidth is limited due to the usually high junction capacitance. Thus, high-power LEDs are limited by output frequency of few tens of Mbps, and very low-power micro-LEDs, although able to achieve high output frequencies, are limited to a range of a few meters [104–107]. Even though the switching-frequency ceiling of high-power LEDs can be raised using pre-emphasis circuitry, orders of Gbps are far out of reach [108]. Furthermore, LEDs emit depolarized beams at wide spectral bandwidths that restrict encoding and channel utilization efficiencies, while coming short of the other advantages posed by higher-order beams towards meeting propagation and multiple access needs previously discussed. It is to this end that laser-based point-to-point (P2P) systems are beneficial, which until recently, have suffered from pointing-

acquisition-and-tracking demands, where, now, employing RIS may be an ideal solution. For example, applications of machine learning in UOWCs have been proposed promisingly in CSI estimation, beam-adaptation, and routing-protocol design, which can be adapted to function with RIS [109–112]. Localization may be achieved simultaneously by assessing the received signal strength indicator (RSSI) at the node or comparing the RSSI of two distinct wavelengths which have undergone spectrally distinct attenuation loss [103]. This way, the RIS-enabled dynamic controllability of narrow-beam-divergent beams outside Snell's laws of reflection and refraction, and conversion of one type and wavelength of beams to another can be packaged with artificial intelligence-optimized decision-making to enhance mobile UOWCs within the time-variant channel (stratified IOPs, ambient light, and turbulence effects, etc.) to ultimately ensure a high SNR signal to always orthogonally incident on the photodetector [103]. All other mobile technologies as usually used with mobile communication can be overlayed upon this architecture.

Such strategies may be beneficial also for multiuser access, where users with distinctive channel conditions can be grouped into a combined set of OMA and/or NOMA schemes. For example, a set of users in the more attenuating and sunlit euphotic zone could be allocated a distinct frequency-domain or PDM-based NOMA scheme at a yellow or amber wavelength [36], while users further below could use blue-green transmissions employing a different NOMA scheme. Spatial modulation could further segregate users who do not share the same line of sight path with the reflector. The RIS for such a system could be placed beneath the DCM, acting as the intermediary between the sunlit and phytoplankton-rich, and the optically clear and dark half spaces. These strategies could be achieved with integrating technologies discussed in Section 2.4. This way, the overall complexity of decoding can be reduced while accommodating more users. Such a system would also reduce potential channel saturation by high-power transmissions, which are commonly suggested for overcoming the higher attenuation effects underwater.

Thus, there is significant theoretical and application-specific research potential for RIS in this area. A UOWC network employing a combination of these technologies is visualized in Figure 13.

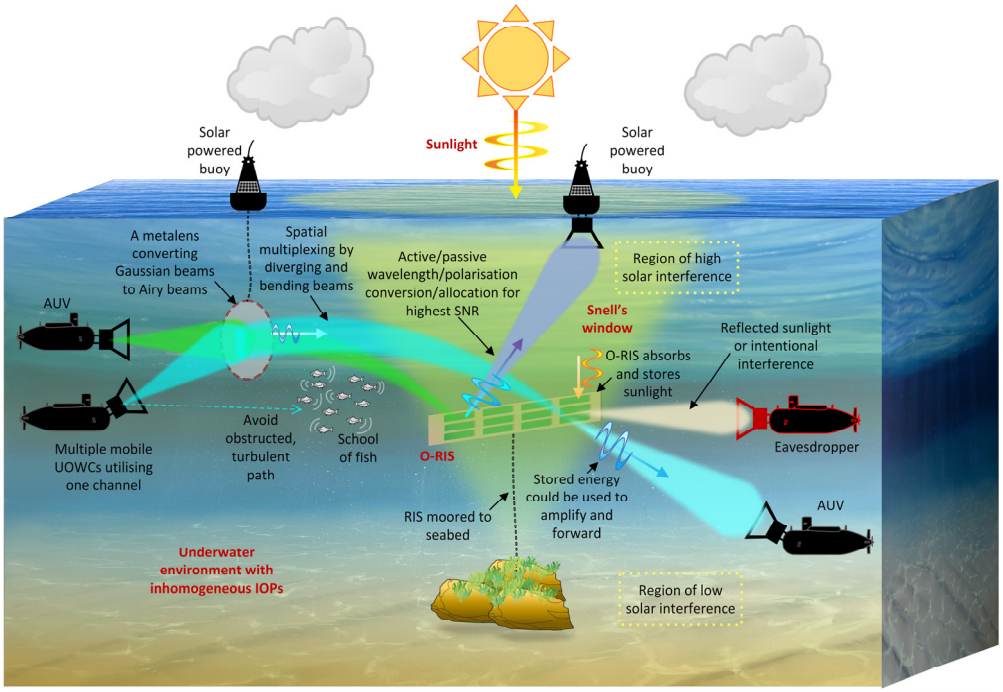

Figure 13. A conceptual UOWC network incorporating known RIS and metasurface strategies for more reliable and secure UOWC connectivity. Arrows show the link direction.

5.3. Wideband Beamforming for A-RIS

UWA has limited bandwidth resources. Using broadband signals, such as multicarrier orthogonal frequency-division multiplexing (OFDM), can transmit more information. Recent research on broadband beamforming for terrestrial EM RIS has also focused on OFDM systems [113]. However, unlike electromagnetic broadband signals, underwater acoustic broadband signals typically have a bandwidth-to-center-frequency ratio of less than 20%. Common reflection design methods based on maximizing the sum rate can, to some extent, mitigate the beam squint effect in the system but fail to fundamentally eliminate this issue, especially in wideband UWA systems.

Deep learning can be introduced to predict time-varying channel states by training neural networks. This allows the RIS to dynamically adjust its reflection characteristics in real time, adapting to the complex broadband signal environment of underwater acoustic channels [110,114]. Further, a codebook generation algorithm based on deep reinforcement learning can be used to generate phase codebooks in real time through gradient optimization. This enables the optimization of reflection paths in dynamic environments [115]. By employing these methods, the RIS can achieve constructive signal superposition for multipath signals, effectively suppress interference while significantly improving the SNR. This, in turn, enhances the overall performance of UWA systems.

5.4. Multiuser Communication and Resource Allocation Optimization in A-RIS

In recent years, multiuser communication has become a critical requirement in the field of the Internet of Underwater Things (IoUT). In multiuser scenarios, interference and channel contention among users severely impact communication efficiency. By intelligently controlling the propagation paths and directions of acoustic waves, RIS provides a new dimension for optimizing underwater multiuser communication. RIS shows significant potential in improving spectrum utilization, enhancing signal quality and coverage, and meeting the differentiated service needs of multiple users.

RIS can generate multiple independent beams to achieve signal separation among users, thereby supporting efficient multiuser communication. By integrating dynamic user scheduling algorithms with beam separation techniques, spectrum allocation can be further optimized to maximize the overall system rate [116], decompose the complex problem into two sub-problems: resource allocation and RIS phase shift optimization under limited resource conditions, the joint optimization of the RIS reflection matrix, and power allocation strategies can significantly enhance spectrum efficiency.

By optimizing RIS reflection path design, differentiated power can be allocated to near-field and far-field users, minimizing interference between users [117]. Furthermore, optimizing the reflection matrix to improve channel gain, combined with efficient coding techniques, such as LDPC and Polar codes, can effectively enhance decoding accuracy and improve overall system performance [118].

Multiagent Deep Reinforcement Learning algorithms provide efficient solutions for resource allocation and beamforming problems [119,120]. By treating each RIS element or user as an independent intelligent agent, collaborative learning can achieve global optimization. This approach not only dynamically adapts to the complexities of underwater channel environments but also significantly improves system performance. Leveraging these intelligent methods, RIS offers promising opportunities to address resource contention and channel interference challenges in multiuser scenarios.

5.5. Implications for RIS Hardware Designs in Seawater

RIS hardware needs to be designed with additional considerations for operability and survivability underwater. Generally, the underwater environment's high pressure,

corrosiveness, and temperature variations demand RIS materials with exceptional pressure resistance, anticorrosion capabilities, and environmental adaptability, while ensuring long-term operational stability [121].

Presently, optical RIS would require that the metamaterials or the reflecting elements be directly exposed to the water. However, deployment durations longer than a few hours, or where devices are not regularly cleaned, will be highly susceptible to biofouling. This is when organisms, such as (initially) microalgae, bacteria and fungi, (later followed by larger) seaweed, bryozoans, and mussels settle on the surfaces compromising their performances. The first condition film would have formed within seconds to minutes post submergence, immediately followed by biofilm, and then macrofouling within less than a day [122]. Adopting preventative measures could be helpful, such as periodic ultraviolet sterilization of the surfaces, integration of metallic biocides, such as copper-based alloy coatings, nanoscale graphene coatings that hinder surface adhesions, or antifouling biomimetic surface coatings and microtopographies, such as those in shark skin [122,123]. Graphene-based metasurfaces may be particularly advantageous, because graphene is also a proven optical metamaterial [4]. Additionally, it is common knowledge that no electrical contact points should be exposed to sea water. Traditionally, where encased housings were not used, the transceivers with surface-mount components have been covered in a layer of epoxy but could have implications for free movement for IRS elements and alter the dielectric performance of metasurfaces [124]. Utilization of flexible material could be ideal such as those based on flexible perovskites [125]. Furthermore, depth- and time-variations of salinity and temperature need to also be considered in selecting or determining the dielectric properties of the RIS structures. Particularly, regarding metasurfaces for UWC, system considerations need to be made whether the elements should be exposed to the water or not. For exposed metasurface designs, the jump in the refractive index underwater needs to be noted, and any variations of the permittivity along the thermo-, halo-, and pycnoclines, also accounting for any spectral shifts of the resonance curves of the RIS elements. Attention should be paid to variations in pressure and buoyant forces, particularly in composite systems, so that the metalenses do not deform and degrade performance. These are crucial considerations for employing metalenses, such as those discussed in Section 2.4, for the generation of Airy beams.

In relation to acoustic RIS, the size and arrangement precision of RIS reflective elements face strict requirements, due to the relatively long wavelength of acoustic waves. Traditional micro-unit designs are often difficult to adapt directly to acoustic characteristics [51]. Additionally, RIS must achieve high-precision control of the phase and amplitude of acoustic waves, making the development of low-power, high-efficiency control circuits a key technical hurdle [126].

Overall, minimal exposure of moving parts or actuators is advised to prevent any catching of debris that could result in damage. Unlike terrestrial deployments where signals may just be reflected from only one half-space, underwater RIS should be able to reflect coming from all directions [1]. Regarding placement, relatively stationery placement is possible by attaching to floating buoy (surface water RIS), to the wall of a fish pen, aquaculture, or other underwater structure at similar depth (mid-water RIS), or moored to the seafloor (bottom water RIS). An unattached, hovering, stationary RIS may also be possible, but would need to perform active station-keeping constantly by monitoring its inertial measurements and updating its buoyancy and thrust forces to prevent unsuspected gradual drift. Nevertheless, such a scheme may compromise the energy advantages of using RIS.

5.6. Acoustic-Optical Hybrid RIS

Underwater wireless communication systems could effectively overcome the limitations of single communication methods by integrating complementary acoustic and optical transmission technologies [127,128]. Currently, underwater acoustic communication dominates long-distance transmission, with frequency ranges reaching tens of kilohertz [129], up to a maximum of 250 kHz [130], offering strong penetration capabilities and interference resistance, though with limited bandwidth and data rates. In contrast, underwater optical communication can achieve high-speed transmission from several megahertz to gigabits per second, but is constrained by water absorption and scattering, typically resulting in shorter transmission distances [99]. The complementary structure where acoustics handles long-distance connectivity while optics assists with high-bandwidth communication provides ideal flexibility for underwater communications, adapting to various marine environments and application requirements. Introducing RIS technology into this joint communication architecture enables dynamic optimization of transmission paths through intelligent reconfiguration of acoustic and optical fields, significantly enhancing system performance. This could be enabled by the fact that the surface elements of acoustic RIS oscillate in the kHz frequency scales, a much lower frequency than what optical RIS would operate with, minimizing the risk of ISI. This way, it may be possible to even create a device that converts between acoustic and optical waves. Such a RIS system could have many advantages:

1. Fewer RIS hardware are needed if one device can service both acoustic and optical links, moving closer to the idealistic vision for underwater connectivity under the 6G package.
2. Congestion in either link type could be reduced by switching to the alternative channel. The RIS devices in between the sender and receiver could thus operate using this optimal mode.
3. There could be improvement in security in selectively choosing the transmission mode. For example, where the receiver and transmitter are close by, establishing a UOWC will ensure it is less likely to be overheard by eavesdroppers beyond the link range due to directionality and attenuation.
4. In environments unfavorable to UOWCs, such as those with high attenuation or significant obstructions, the links could instead be established as UWACs, to ensure reliability.
5. In environments unfavorable for UWACs, such as in spatially narrow channels that induce multipath effects, shifting to UOWCs may achieve better performance.
6. Improved energy efficiency overall. For example, given that UOWCs are more energy efficient per data bit overall, compared to UWACs, and given that RIS facilitates targeted, high-SNR links to be established, a long-distance acoustic transmission converted to optical signals and reflected within a local network may be more energy efficient than a fully acoustic one.
7. Enhanced reliability and robustness, because there is an alternative mode in the event one form of communication becomes impaired.

The energy to realize this could be possible by integrating energy harvesting technologies with RIS. In addition to the previously discussed optical energy harvesting methods, such as from sunlight, research [131,132] shows that mechanical energy from acoustic wave propagation can be converted to electrical energy through piezoelectric materials. These could utilize the same RIS element structures, when there is no ongoing communication. This way, RIS surfaces can be simultaneously configured with acoustic and optical energy collection units, forming self-sustainable communication systems.

As such, an underwater hybrid RIS fusion system can enhance the flexibility of distributed RIS networks, forming long-distance, high-bandwidth underwater communication networks through energy harvesting, and intelligent reflection and relaying. Environment-aware adaptive switching mechanisms that intelligently select optimal transmission modes based on water conditions will significantly improve the flexibility, reliability, and energy efficiency of underwater communication systems.

6. Conclusions

This article presented a thorough survey of the current state-of-the-art in the application of underwater wireless technologies. Acoustic and optical wireless technologies were the main areas investigated with a keen interest in uncovering the potential areas of future research and development involving RIS.

The inherent time-varying nature of UWAC, particularly the significant multipath and Doppler effects, poses a core challenge to the application of A-RIS. Due to the wideband characteristics of UWA signals, A-RIS must overcome the Doppler squint effect phenomenon induced by Doppler shifts during beamforming, which necessitates the design of advanced wideband beamforming algorithms to ensure signal processing accuracy. In severely band-limited underwater multiuser communication scenarios, leveraging A-RIS to effectively suppress interference and enhance spectral efficiency remains a critical research direction for achieving high-performance communication. Furthermore, the hardware design of A-RIS must fully account for the stringent demands of the complex underwater environment, achieving low power consumption, high efficiency, miniaturization, and robust system integration to ensure its practical deployability and long-term operational reliability.

With UOWCs, some of the current research challenges revolve around overcoming the drastic effects of the medium in terms of inhomogeneity, solar interference, turbulence, etc. To this end, it may be beneficial to incorporate higher-order beams that are more resistant to these effects, which can be achieved by a combination of metasurface and RIS technologies. For example, the latest developments suggest that self-powered RIS may be possible (powered by sunlight or stray signals), that convert Gaussian beams to more complex ones, and/or reflect only certain polarizations of light, which are more resistant to solar interference under strong sunlight. Additionally, from a networking perspective, RIS and metasurfaces may be used to tweak transmission parameters between intermediate nodes to always enable the highest-SNR link, which may be contingent on the medium condition along the route path. Such adaptive approaches may also be used to improve link security by enhancing channel entropy and reciprocity between intended sender and receiver. Finally, the challenges and opportunities in realizing the hardware underwater were discussed, where exposed mechanical systems are unideal, and performance of optically sensitive material may degrade overtime as a result of biofouling.

Overall, the future directions could prioritize developing dynamic, low-power RIS for significant enhancements in UWC, boosting data rates and range for autonomous systems. The integration of machine learning for real-time control and the exploration of novel materials could unlock the full potential of this transformative technology.

Author Contributions: Conceptualization, T.G.W. and B.-C.S.; methodology, T.G.W., Y.Y., and B.-C.S.; software, T.G.W. and Y.Y.; validation, T.G.W. and Y.Y.; formal analysis, T.G.W. and Y.Y.; investigation, T.G.W. and Y.Y.; resources, B.-C.S.; data curation, T.G.W. and Y.Y.; writing—original draft preparation, T.G.W. and Y.Y.; writing—review and editing, T.G.W., Y.Y., and B.-C.S.; visualization, T.G.W. and B.-C.S.; supervision, B.-C.S.; project administration, B.-C.S.; funding acquisition, T.G.W. and B.-C.S. All authors have read and agreed to the published version of the manuscript.

Funding: This research received no external funding.

Data Availability Statement: Data are available in the manuscript.

Acknowledgments: We would like to thank Kay Vopel and the School of Science at Auckland University of Technology, for their resources and facilitation of the voyage out to the sea, during which the data presented in Figure 9 were collected.

Conflicts of Interest: The authors declare no conflicts of interest.

Abbreviations

The following abbreviations are used in this manuscript:

AF	Amplify and Forward
AI	Artificial Intelligence
AN	Artificial Noise
A-RIS	Acoustic Reconfigurable Intelligent Surfaces
ASC	Average Secrecy Capacity
ASE	Average Spectral Efficiency
AUV	Autonomous Underwater Vehicles
BER	Bit Error Rates
BFSK	Binary Frequency Shift Keying
BPSK	Binary Phase Shift Keying
CAFAB	Circular Autofocusing
CBFSK	Coherent Binary Frequency Shift Keying
CBPSK	Coherent Binary Phase Shift Keying
CC	Channel Capacity
CDOM	Colored Dissolved Organic Matter
CIR	Channel Impulse Response
CSI	Channel State Information
CTD	Conductivity, Temperature, and Depth
DBPSK	Differential Binary Phase Shift Keying
DCM	Deep-Chlorophyll Maximum
DF	Decode and Forward
DMA	Distance-Based Mirror Assignment
EMA	Equal Mirror Assignment
EST	Effective Secrecy Throughput
FSO	Free-Space Optical Communication
HAPS	High-Altitude Platform Station
HD	Heterodyne
IMDD	Intensity Modulation Direct Detection
IOPs	Inherent Optical Properties
IoUT	Internet Of Underwater Things
ISI	Intersymbol Interference
LED	Light-Emitting Diode
LOS	Line Of Sight
LQAM-MPPM	L-Ary Quadrature Amplitude Modulation Multipulse Pulse-Position Modulation
MC	Monte-Carlo
MCUs	Microcontroller Unit
mEGG	Mixture Exponential Generalized Gamma distribution
ML-ARIS	Multilayer Acoustic Reconfigurable Intelligent Surface
MRR	Modulating Retroreflector
NCBFSK	Non-Coherent Binary Frequency Shift Keying
NCBPSK	Non-Coherent Binary Phase Shift Keying
NLOS	Non-Line-Of-Sight
OFDM	Orthogonal Frequency Division Multiplexing

OIRS	Optical Intelligent Reflecting Surface
OMA	Orthogonal Multiple Access
OOK	On-Off Keying
OP	Outage Probability
O-RIS	Optical Reconfigurable Intelligent Surfaces
OSNR	Optical Signal-to-Noise Ratio
OTOPS	Oceanic Turbulence Optical Power Spectrum
P2P	Point-To-Point
PDM	Polarization Division Multiplexing
PMS	Planar Mirror-Array Surface
PZT	Multiple Piezoelectric Ceramic
QAM	Quadrature Amplitude Modulation
RF	Radiofrequency
RGB	Red, Green, Blue
RIS	Reconfigurable Intelligent Surfaces
ROP	Received Optical Power
RSMA	Rate-Split Multiple Access
RSSI	Received Signal Strength Indicator
SA-RIS	Security-Based Adaptive Reconfigurable Intelligent Surface
SIMO	Single Input Multiple Output
SiPM	Silicon Photomultiplier
SISO	Single-Input Single-Output
SNR	Signal-To-Noise Ratio
SOP	Secrecy Outage Probability
SPAD	Single-Photon Avalanche Photodiode
SPP	Surface Plasmon Polariton
SPSC	Strictly Positive Secrecy Capacity
STAR	Simultaneous Transmit and Reflect
TIR	Total Internal Reflection
UAV	Unmanned Aerial Vehicle
UOWC	Underwater Optical Wireless Communication
UWAC	Underwater Acoustic Communication
UWC	Underwater Wireless Communication
VLC	Visible Light Communication
WDM	Wavelength Division Multiplexing

References

1. Kisseleff, S.; Chatzinotas, S.; Ottersten, B. Reconfigurable intelligent surfaces in challenging environments: Underwater, underground, industrial and disaster. *IEEE Access* **2021**, *9*, 150214–150233. [CrossRef]
2. Kaushal, H.; Kaddoum, G. Underwater Optical Wireless Communication. *IEEE Access* **2016**, *4*, 1518–1547. [CrossRef]
3. Abumarshoud, H.; Mohjazi, L.; Dobre, O.A.; Di Renzo, M.; Imran, M.A.; Haas, H. LiFi through reconfigurable intelligent surfaces: A new frontier for 6G? *IEEE Veh. Technol. Mag.* **2021**, *17*, 37–46. [CrossRef]
4. Aboagye, S.; Ndjiongue, A.R.; Ngatched, T.M.; Dobre, O.A.; Poor, H.V. RIS-assisted visible light communication systems: A tutorial. *IEEE Commun. Surv. Tutor.* **2022**, *25*, 251–288. [CrossRef]
5. Sun, S.; Wang, T.; Yang, F.; Song, J.; Han, Z. Intelligent reflecting surface-aided visible light communications: Potentials and challenges. *IEEE Veh. Technol. Mag.* **2021**, *17*, 47–56. [CrossRef]
6. Fang, C.; Li, S.; Wang, Y.; Wang, K. Survey on Optical Wireless Communication with Intelligent Reflecting Surfaces. *Photonics* **2024**, *11*, 830. [CrossRef]
7. Horsley, S.; Woolley, M. Zero-refractive-index materials and topological photonics. *Nat. Phys.* **2021**, *17*, 348–355. [CrossRef]
8. Ndjiongue, A.R.; Ngatched, T.M.; Dobre, O.A.; Haas, H. Re-configurable intelligent surface-based VLC receivers using tunable liquid-crystals: The concept. *J. Light. Technol.* **2021**, *39*, 3193–3200. [CrossRef]
9. Li, Y.; Li, X.; Chen, L.; Pu, M.; Jin, J.; Hong, M.; Luo, X. Orbital angular momentum multiplexing and demultiplexing by a single metasurface. *Adv. Opt. Mater.* **2017**, *5*, 1600502. [CrossRef]

10. Díaz-Rubio, A.; Asadchy, V.S.; Elsakka, A.; Tretyakov, S.A. From the generalized reflection law to the realization of perfect anomalous reflectors. *Sci. Adv.* **2017**, *3*, e1602714. [CrossRef]
11. Abdelhady, A.M.; Salem, A.K.S.; Amin, O.; Shihada, B.; Alouini, M.-S. Visible light communications via intelligent reflecting surfaces: Metasurfaces vs mirror arrays. *IEEE Open J. Commun. Soc.* **2020**, *2*, 1–20. [CrossRef]
12. Naik, R.P.; Chung, W.-Y. Evaluation of reconfigurable intelligent surface-assisted underwater wireless optical communication system. *J. Light. Technol.* **2022**, *40*, 4257–4267. [CrossRef]
13. Ata, Y.; Abumarshoud, H.; Bariah, L.; Muhaidat, S.; Imran, M.A. Intelligent reflecting surfaces for underwater visible light communications. *IEEE Photonics J.* **2023**, *15*, 1–10. [CrossRef]
14. Haltrin, V.I. Chlorophyll-based model of seawater optical properties. *Appl. Opt.* **1999**, *38*, 6826–6832. [CrossRef] [PubMed]
15. Lam, V.T.; Van Thang, N.; Sy, T.D.; Ngoc, D.T.; Anh, D.T. Outage Performance of IRS-Assisted Underwater Optical Wireless Communication Systems over Combined Channel Model. In *Proceedings of the 2023 19th International Conference on Wireless and Mobile Computing, Networking and Communications (WiMob), Montreal, QC, Canada, 21–23 June 2023*; IEEE: New York, NY, USA, 2023; pp. 318–323.
16. Ata, Y.; Gökçe, M.C.; Baykal, Y. Intelligent Reflecting Surface Aided Vehicular Optical Wireless Communication Systems using Higher-order Mode in Underwater Channel. *IEEE Trans. Veh. Technol.* **2024**, *73*, 11196–11208. [CrossRef]
17. Salam, R.; Srivastava, A.; Bohara, V.A.; Ashok, A. An optical intelligent reflecting surface-assisted underwater wireless communication system. *IEEE Open J. Commun. Soc.* **2023**, *4*, 1774–1786. [CrossRef]
18. Gan, Z.; Cox, M.; Dong, Y. On RIS-aided NLOS Underwater Wireless Optical Communication Systems. In *Proceedings of the 2024 Photonics & Electromagnetics Research Symposium (PIERS), Chengdu, China, 21–25 April 2024*; IEEE: New York, NY, USA, 2024; pp. 1–7.
19. Wei, Z.; Wei, Z.; Fang, J.; Pan, J.; Wang, L.; Dong, Y. Impulse Response Modeling and Dynamic Analysis for SIMO UOWC Systems Enhanced by RIS-Equipped UUV. *IEEE Trans. Veh. Technol.* **2023**, *73*, 1540–1553. [CrossRef]
20. Zhang, Q.; Yue, D.-W.; Xu, X.-Y. Performance Analysis of Reconfigurable Intelligent Surface-Assisted Underwater Wireless Optical Communication Systems. *IEEE Photonics J.* **2024**, *16*, 7301914. [CrossRef]
21. Odeyemi, K.O.; Owolawi, P.A.; Olakanmi, O.O. Performance analysis of reconfigurable intelligent surface assisted underwater optical communication system. *Prog. Electromagn. Res. M* **2020**, *98*, 101–111. [CrossRef]
22. Zedini, E.; Oubei, H.M.; Kammoun, A.; Hamdi, M.; Ooi, B.S.; Alouini, M.-S. Unified statistical channel model for turbulence-induced fading in underwater wireless optical communication systems. *IEEE Trans. Commun.* **2019**, *67*, 2893–2907. [CrossRef]
23. Li, S.; Yang, L.; da Costa, D.B.; Di Renzo, M.; Alouini, M.-S. On the performance of RIS-assisted dual-hop mixed RF-UWOC systems. *IEEE Trans. Cogn. Commun. Netw.* **2021**, *7*, 340–353. [CrossRef]
24. Salam, R.; Srivastava, A.; Bohara, V.A.; Ashok, A. Performance Comparison of IRS and DF Relay Assisted Mixed RF-Underwater Optical Communication System. In *Proceedings of the 2022 IEEE International Conference on Advanced Networks and Telecommunications Systems (ANTS), Gandhinagar, India, 18–21 December 2022*; IEEE: New York, NY, USA, 2022; pp. 129–134.
25. Kumar, L.B.; Naik, R.P.; Krishnan, P.; Raj, A.A.B.; Majumdar, A.K.; Chung, W.-Y. RIS assisted triple-hop RF-FSO convergent with UWOC system. *IEEE Access* **2022**, *10*, 66564–66575. [CrossRef]
26. Ramavath, P.N.; Chung, W.-Y. Performance evaluation of re-configurable intelligent surface-assisted underwater and free-space wireless optical communication in the skip-zones. *ICT Express* **2024**, *10*, 320–329. [CrossRef]
27. Rakib, M.A.; Ibrahim, M.; Badrudduza, A.S.M.; Ansari, I.S.; Chakravarty, S.; Ahmed, I. A RIS empowered THz-UWO relay system for air-to-underwater mixed network: Performance analysis with pointing errors. *IEEE Internet Things J.* **2024**, *11*, 17097–17112. [CrossRef]
28. Deka, R.; Alam, M.S.; Ahmed, I.; Anees, S. Performance Analysis of a RIS-HAPS Assisted FSO-UWOC System for Ground-Air-Underwater Connectivity. In *Proceedings of the 2024 IEEE 100th Vehicular Technology Conference (VTC2024-Fall), Washington, DC, USA, 7–10 October 2024*; IEEE: New York, NY, USA, 2024; pp. 1–5.
29. Elsayed, M.; Samir, A.; El-Banna, A.A.A.; Khan, W.U.; Chatzinotas, S.; ElHalawany, B.M. Mixed RIS-Relay NOMA-Based RF-UOWC Systems. In *Proceedings of the 2022 IEEE 95th Vehicular Technology Conference:(VTC2022-Spring), Helsinki, Finland, 19–22 June 2022*; IEEE: New York, NY, USA, 2022; pp. 1–6.
30. Hossain, T.; Shabab, S.; Badrudduza, A.; Kundu, M.K.; Ansari, I.S. On the physical layer security performance over RIS-aided dual-hop RF-UOWC mixed network. *IEEE Trans. Veh. Technol.* **2022**, *72*, 2246–2257. [CrossRef]
31. Sarawar, A.B.; Badrudduza, A.; Ibrahim, M.; Ansari, I.S.; Yu, H. Secrecy Performance Analysis of Integrated RF-UOWC IoT Networks Enabled by UAV and Underwater-RIS. *IEEE Internet Things J.* **2024**, *12*, 2592–2608. [CrossRef]
32. Dang, T.S.; Van Toan, C.; Nguyen, T.V.; Dang, N. Secrecy performance analysis of a IRS-assisted underwater optical wireless communication system. *J. Mil. Sci. Technol.* **2024**, *96*, 21–29. [CrossRef]
33. Tian, Y.; Zheng, X. A novel security-based adaptive reconfigurable intelligent surfaces assisted clustering strategy. *Electron. Lett.* **2024**, *60*, e70008. [CrossRef]

34. Salam, R.; Bohara, V.A.; Srivastava, A. Smart Element Allocation Strategies for Dynamic Optical IRS in Underwater Wireless Communication. *IEEE Trans. Veh. Technol.* **2024**, *74*, 4349–4361. [CrossRef]
35. Uitz, J.; Claustre, H.; Morel, A.; Hooker, S.B. Vertical distribution of phytoplankton communities in open ocean: An assessment based on surface chlorophyll. *J. Geophys. Res. Oceans* **2006**, *111*, C08005. [CrossRef]
36. Waduge, T.G.; Seet, B.-C.; Vopel, K. Optimal Signal Wavelengths for Underwater Optical Wireless Communication under Sunlight in Stratified Waters. *J. Sens. Actuator Netw.* **2024**, *13*, 54. [CrossRef]
37. Naik, R.P.; Salman, M.; Bolboli, J.; Shetty, S.; Chung, W.-Y. Multiuser data transmission aided by simultaneous transmit and reflect reconfigurable intelligent surface in underwater wireless optical communications. *IEEE Trans. Veh. Technol.* **2024**, *73*, 8420–8433. [CrossRef]
38. Benea-Chelmus, I.-C.; Meretska, M.L.; Elder, D.L.; Tamagnone, M.; Dalton, L.R.; Capasso, F. Electro-optic spatial light modulator from an engineered organic layer. *Nat. Commun.* **2021**, *12*, 5928. [CrossRef]
39. Matsuo, T.; Mizuno, H.; Sasaki, F.; Yanagi, H. Indication of cooperative light amplification in 5,5″-bis (4-biphenylyl)-2,2′:5,2″-terthiophene single crystals at room temperature. *Jpn. J. Appl. Phys.* **2019**, *59*, SDDB02. [CrossRef]
40. AbdElKader, A.G.; Allam, A.; Kato, K.; Shalaby, H.M. Performance enhancement of RIS-assisted MRR-UOWC systems using the spectral-power-efficient LQAM-MPPM. *Opt. Commun.* **2024**, *559*, 130444. [CrossRef]
41. Zhao, F.; Lu, R.; Chen, X.; Jin, C.; Chen, S.; Shen, Z.; Zhang, C.; Yang, Y. Metalens-assisted system for underwater imaging. *Laser Photonics Rev.* **2021**, *15*, 2100097. [CrossRef]
42. Ren, Y.; Li, L.; Wang, Z.; Kamali, S.M.; Arbabi, E.; Arbabi, A.; Zhao, Z.; Xie, G.; Cao, Y.; Ahmed, N.; et al. Orbital angular momentum-based space division multiplexing for high-capacity underwater optical communications. *Sci. Rep.* **2016**, *6*, 33306. [CrossRef]
43. Hu, J.; Guo, Z.; Shi, J.; Jiang, X.; Chen, Q.; Chen, H.; He, Z.; Song, Q.; Xiao, S.; Yu, S.; et al. A metasurface-based full-color circular auto-focusing Airy beam transmitter for stable high-speed underwater wireless optical communications. *Nat. Commun.* **2024**, *15*, 2944. [CrossRef]
44. Geng, J. Structured-light 3D surface imaging: A tutorial. *Adv. Opt. Photonics* **2011**, *3*, 128–160. [CrossRef]
45. Efremidis, N.K.; Chen, Z.; Segev, M.; Christodoulides, D.N. Airy beams and accelerating waves: An overview of recent advances. *Optica* **2019**, *6*, 686–701. [CrossRef]
46. Wang, J.; Wang, X.; Peng, Q.; Zhao, S. Propagation characteristics of autofocusing Airy beam with power exponential phase vortex in weak anisotropic oceanic turbulence. *J. Mod. Opt.* **2021**, *68*, 1059–1065. [CrossRef]
47. Zhang, X.G.; Sun, Y.L.; Zhu, B.; Tian, H.W.; Wang, B.Y.; Zhang, Z.; Qiu, C.-W.; Cui, T.J.; Jiang, W.X. Wireless microwave-to-optical conversion via programmable metasurface without DC supply. *Nat. Commun.* **2025**, *16*, 528. [CrossRef]
48. Choi, K.-H.; Choi, J.W.; Kim, S.; Dahl, P.H.; Dall'Osto, D.; Song, H. Experimental Study on Performance Improvement of Underwater Acoustic Communication Using a Single Vector Sensor. *IEEE J. Ocean. Eng.* **2024**, *49*, 1574–1587. [CrossRef]
49. Liao, Y.; Zhai, N.; Song, Y.; Wang, H.; Han, Y.; Xu, N. Performance Analysis of Acoustic RIS-Assisted Wireless Underwater Communications. In Proceedings of the 2024 IEEE 99th Vehicular Technology Conference (VTC2024-Spring), Singapore, 24–27 June 2024; pp. 1–5. [CrossRef]
50. Sun, Z.; Guo, H.; Akyildiz, I.F. High-Data-Rate Long-Range Underwater Communications via Acoustic Reconfigurable Intelligent Surfaces. *IEEE Commun. Mag.* **2022**, *60*, 96–102. [CrossRef]
51. Wang, H.; Sun, Z.; Guo, H.; Wang, P.; Akyildiz, I.F. Designing Acoustic Reconfigurable Intelligent Surface for Underwater Communications. *IEEE Trans. Wirel. Commun.* **2023**, *22*, 8934–8948. [CrossRef]
52. Edemen, C.; Altabbaa, M.T.; Uysal, M. Channel Modeling of Reconfigurable Intelligent Surface-aided Underwater Acoustic Communication System. In Proceedings of the 2024 32nd Signal Processing and Communications Applications Conference (SIU), Mersin, Turkiye, 15–18 May 2024; pp. 1–3. [CrossRef]
53. Silva, A.; Zabel, F.; Martins, C.; Ijaz, S.; Jesus, S. An environmental equalizer for underwater acoustic communications Tested at Hydralab III. In *Hydralab III Joint User Meeting*; Coastal Research Centre FZK, University of Hannover: Hannover, Germany; Technical University Braunschweigh: Braunschweig, Germany, 2010.
54. Song, H. Bidirectional equalization for underwater acoustic communication. *J. Acoust. Soc. Am.* **2012**, *131*, EL342–EL347. [CrossRef]
55. Li, B.; Huang, J.; Zhou, S.; Ball, K.; Stojanovic, M.; Freitag, L.; Willett, P. MIMO-OFDM for high-rate underwater acoustic communications. *IEEE J. Ocean. Eng.* **2009**, *34*, 634–644.
56. Zhou, M.; Zhang, H.; Lv, T.; Gao, Y.; Duan, Y. Spatial diversity processing mechanism based on the distributed underwater acoustic communication system. *PLoS ONE* **2024**, *19*, e0296117. [CrossRef]
57. Zhao, L.; Tan, J.; Wang, J.; Akyildiz, I.F.; Sun, Z. Covering Underwater Shadow Zones using Acoustic Reconfigurable Intelligent Surfaces. *arXiv* **2025**, arXiv:250102256. [CrossRef]

58. Dong, Y.; Chen, Z.; Song, Z.; Chen, Y.; Zhang, X. Reconfigurable Intelligent Surface Transmission for Data Importance Classification in Underwater Acoustic Networks with Energy Holes. In Proceedings of the 2023 IEEE International Conference on Signal Processing, Communications and Computing (ICSPCC), Zhengzhou, China, 14–17 November 2023; pp. 1–4. [CrossRef]
59. Luo, Y.; Pu, L.; Song, A. Experimental Study of Underwater Acoustic Reconfigurable Intelligent Surfaces with In-Phase and Quadrature Modulation. *arXiv* **2024**, arXiv:241112906. [CrossRef]
60. Chen, Z.; Du, J.; Jiang, C.; Han, Z. Joint Optimization of Communication Enhancement and Location Privacy Protection in RIS-Assisted Underwater Communication System. *arXiv* **2024**, arXiv:241200367. [CrossRef]
61. Luo, Y.; Pu, L.; Diao, J.; Liu, C.-H.; Song, A. Underwater Acoustic Reconfigurable Intelligent Surfaces: From Principle to Practice. *arXiv* **2024**, arXiv:241217865. [CrossRef]
62. Kameda, T.; Matsumura, S. Chlorophyll biomass off Sanriku, northwestern Pacific, estimated by Ocean Color and Temperature Scanner (OCTS) and a vertical distribution model. *J. Oceanogr.* **1998**, *54*, 509–516. [CrossRef]
63. Johnson, L.J.; Green, R.J.; Leeson, M.S. Underwater optical wireless communications: Depth dependent variations in attenuation. *Appl. Opt.* **2013**, *52*, 7867–7873. [CrossRef]
64. Duntley, S.Q. Light in the sea. *JOSA* **1963**, *53*, 214–233. [CrossRef]
65. Bird, R.E.; Riordan, C. Simple solar spectral model for direct and diffuse irradiance on horizontal and tilted planes at the earth's surface for cloudless atmospheres. *J. Appl. Meteorol. Climatol.* **1986**, *25*, 87–97. [CrossRef]
66. NREL SMARTS: Simple Model of the Atmospheric Radiative Transfer of Sunshine. Available online: https://www.nrel.gov/grid/solar-resource/smarts.html (accessed on 21 August 2024).
67. Gueymard, C. *SMARTS2: A Simple Model of the Atmospheric Radiative Transfer of Sunshine: Algorithms and Performance Assessment*; Florida Solar Energy Center: Cocoa, FL, USA, 1995; Volume 1.
68. Spectral Sciences Inc. MODTRAN®. Available online: http://modtran.spectral.com/ (accessed on 21 August 2024).
69. Sticklus, J.; Hieronymi, M.; Hoeher, P.A. Effects and constraints of optical filtering on ambient light suppression in LED-based underwater communications. *Sensors* **2018**, *18*, 3710. [CrossRef] [PubMed]
70. Waduge, T.G.; Seet, B.-C.; Vopel, K. Modeling Ambient Light in Stratified Waters for Underwater Optical Wireless Communication. In Proceedings of the 2024 IEEE 99th Vehicular Technology Conference (VTC2024-Spring), Singapore, 24–27 June 2024; pp. 1–6. [CrossRef]
71. Cronin, T.W.; Marshall, J. Patterns and properties of polarized light in air and water. *Philos. Trans. R. Soc. B Biol. Sci.* **2011**, *366*, 619–626. [CrossRef] [PubMed]
72. Cheng, H.; Chu, J.; Zhang, R.; Tian, L.; Gui, X. Turbid underwater polarization patterns considering multiple Mie scattering of suspended particles. *Photogramm. Eng. Remote Sens.* **2020**, *86*, 737–743. [CrossRef]
73. Cheng, H.; Chu, J.; Zhang, R.; Tian, L.; Gui, X. Underwater polarization patterns considering single Rayleigh scattering of water molecules. *Int. J. Remote Sens.* **2020**, *41*, 4947–4962. [CrossRef]
74. Marshall, N.J.; Powell, S.B.; Cronin, T.W.; Caldwell, R.L.; Johnsen, S.; Gruev, V.; Chiou, T.-H.S.; Roberts, N.W.; How, M.J. Polarisation signals: A new currency for communication. *J. Exp. Biol.* **2019**, *222*, jeb134213. [CrossRef]
75. Raihan, A.J.; Abas, P.E.; De Silva, L.C. Review of underwater image restoration algorithms. *IET Image Process.* **2019**, *13*, 1587–1596. [CrossRef]
76. Mullen, L.; Cochenour, B.; Rabinovich, W.; Mahon, R.; Muth, J. Backscatter suppression for underwater modulating retroreflector links using polarization discrimination. *Appl. Opt.* **2009**, *48*, 328–337. [CrossRef]
77. Vasilkov, A.P.; Goldin, Y.A.; Gureev, B.A.; Hoge, F.E.; Swift, R.N.; Wright, C.W. Airborne polarized lidar detection of scattering layers in the ocean. *Appl. Opt.* **2001**, *40*, 4353–4364. [CrossRef]
78. Cheng, H.; Zhang, Q.; Wan, Z.; Zhang, Z.; Qin, J. Study on the polarization pattern induced by wavy water surfaces. *Remote Sens.* **2023**, *15*, 4565. [CrossRef]
79. Molkov, A.A.; Dolin, L.S. The Snell's window image for remote sensing of the upper sea layer: Results of practical application. *J. Mar. Sci. Eng.* **2019**, *7*, 70. [CrossRef]
80. Lewis, G.D.; Jordan, D.L.; Roberts, P.J. Backscattering target detection in a turbid medium by polarization discrimination. *Appl. Opt.* **1999**, *38*, 3937–3944. [CrossRef] [PubMed]
81. Zhang, Y.; Wang, Y.; Huang, A.; Hu, X. Effect of underwater suspended particles on the transmission characteristics of polarized lasers. *JOSA A* **2019**, *36*, 61–70. [CrossRef] [PubMed]
82. Korotkova, O. Light propagation in a turbulent ocean. In *Progress in Optics*; Elsevier: Amsterdam, The Netherlands, 2019; Volume 64, pp. 1–43.
83. Baykal, Y.; Ata, Y.; Gökçe, M.C. Underwater turbulence, its effects on optical wireless communication and imaging: A review. *Opt. Laser Technol.* **2022**, *156*, 108624. [CrossRef]
84. Zhang, J.; Zhang, L.; Zhang, A.; Zhang, L.; Li, D.; Zhang, X. Improving the Estimation of Temperature and Salinity by Assimilation of Observed Sound Speed Profiles. *J. Atmospheric Ocean. Technol.* **2021**, *38*, 1277–1289. [CrossRef]
85. Thorsos, E.I. Acoustic scattering from a "'Pierson–Moskowitz'" sea surface. *J. Acoust. Soc. Am.* **1990**, *88*, 335–349. [CrossRef]

86. Higgins, A.; Siderius, M. Acoustic scattering from dynamic rough ocean surfaces using finite-difference time-domain modeling techniques. *J. Acoust. Soc. Am.* **2022**, *152*, A252–A253. [CrossRef]
87. Sun, D.; Wu, J.; Hong, X.; Liu, C.; Cui, H.; Si, B. Iterative double-differential direct-sequence spread spectrum reception in underwater acoustic channel with time-varying Doppler shifts. *J. Acoust. Soc. Am.* **2023**, *153*, 1027–1041. [CrossRef]
88. Badiey, M.; Wan, L.; Escobar-Amado, C.D. Frequency dependent effects of environmental parameters on the broadband acoustic wave propagation in shallow water waveguides. *J. Acoust. Soc. Am.* **2023**, *154*, A134. [CrossRef]
89. Webb, P. *Introduction to Oceanography*; Roger Williams University: Bristol, RI, USA, 2021.
90. Lin, B.; Tang, X.; Ghassemlooy, Z.; Li, Y.; Zhang, M.; Wu, Y.; Li, H. A NOMA scheme for visible light communications with single carrier transmission and frequency-domain successive interference cancellation. *Optik* **2019**, *183*, 445–450. [CrossRef]
91. Li, G.; Zhang, S.; Zentgraf, T. Nonlinear photonic metasurfaces. *Nat. Rev. Mater.* **2017**, *2*, 17010. [CrossRef]
92. Wang, C.; Wen, Y.; Sun, J.; Zhou, J. Recent progress on optical frequency conversion in nonlinear metasurfaces and nanophotonics. *ES Mater. Manuf.* **2022**, *17*, 1–13. [CrossRef]
93. Gao, J.; Vincenti, M.A.; Frantz, J.; Clabeau, A.; Qiao, X.; Feng, L.; Scalora, M.; Litchinitser, N.M. All-optical tunable wavelength conversion in opaque nonlinear nanostructures. *Nanophotonics* **2022**, *11*, 4027–4035. [CrossRef] [PubMed]
94. Ding, F.; Deshpande, R.; Bozhevolnyi, S.I. Bifunctional gap-plasmon metasurfaces for visible light: Polarization-controlled unidirectional surface plasmon excitation and beam steering at normal incidence. *Light Sci. Appl.* **2018**, *7*, 17178. [CrossRef]
95. Ueno, K.; Oshikiri, T.; Sun, Q.; Shi, X.; Misawa, H. Solid-state plasmonic solar cells. *Chem. Rev.* **2017**, *118*, 2955–2993. [CrossRef]
96. Zhu, W.; Fan, Y.; Yang, R.; Geng, G.; Fu, Q.; Gu, C.; Li, J.; Zhang, F. Polarization-multiplexed silicon metasurfaces for multi-channel visible light modulation. *Adv. Funct. Mater.* **2022**, *32*, 2200013. [CrossRef]
97. Qian, Z.; Tian, S.; Zhou, W.; Wang, J.; Guo, H.; Zhuang, S. Polarization-modulated broadband achromatic bifunctional metasurface in the visible light. *Opt. Express* **2023**, *31*, 10905–10917. [CrossRef]
98. Giuliano, G.; Laycock, L.; Rowe, D.; Kelly, A.E. Solar rejection in laser based underwater communication systems. *Opt. Express* **2017**, *25*, 33066–33077. [CrossRef]
99. Ali, M.F.; Jayakody, D.N.K.; Li, Y. Recent trends in underwater visible light communication (UVLC) systems. *IEEE Access* **2022**, *10*, 22169–22225. [CrossRef]
100. Zhao, S.; Zhang, W.; Wang, L.; Li, W.; Gong, L.; Cheng, W.; Chen, H.; Gruska, J. Propagation and self-healing properties of Bessel-Gaussian beam carrying orbital angular momentum in an underwater environment. *Sci. Rep.* **2019**, *9*, 2025. [CrossRef] [PubMed]
101. Khonina, S.N.; Kazanskiy, N.L.; Karpeev, S.V.; Butt, M.A. Bessel beam: Significance and applications—A progressive review. *Micromachines* **2020**, *11*, 997. [CrossRef] [PubMed]
102. Arnon, S. Underwater optical wireless communication network. *Opt. Eng.* **2010**, *49*, 015001. [CrossRef]
103. Waduge, T.G.; Seet, B.-C.; Vopel, K. Geometric Implications of Photodiode Arrays on Received Power Distribution in Mobile Underwater Optical Wireless Communication. *Sensors* **2024**, *24*, 3490. [CrossRef]
104. Hoeher, P.A.; Sticklus, J.; Harlakin, A. Underwater Optical Wireless Communications in Swarm Robotics: A Tutorial. *IEEE Commun. Surv. Tutor.* **2021**, *23*, 2630–2659. [CrossRef]
105. Lin, R.; Liu, X.; Zhou, G.; Qian, Z.; Cui, X.; Tian, P. InGaN micro-LED array enabled advanced underwater wireless optical communication and underwater charging. *Adv. Opt. Mater.* **2021**, *9*, 2002211. [CrossRef]
106. Tian, P.; Liu, X.; Yi, S.; Huang, Y.; Zhang, S.; Zhou, X.; Hu, L.; Zheng, L.; Liu, R. High-speed underwater optical wireless communication using a blue GaN-based micro-LED. *Opt. Express* **2017**, *25*, 1193–1201. [CrossRef]
107. Zhang, M.; Zhou, H. Real-time underwater wireless optical communication system based on leds and estimation of maximum communication distance. *Sensors* **2023**, *23*, 7649. [CrossRef] [PubMed]
108. Zhou, H.; Zhang, M.; Wang, X.; Ren, X. Design and implementation of more than 50m real-time underwater wireless optical communication system. *J. Light. Technol.* **2022**, *40*, 3654–3668. [CrossRef]
109. Romdhane, I.; Kaddoum, G. A Reinforcement-Learning-Based Beam Adaptation for Underwater Optical Wireless Communications. *IEEE Internet Things J.* **2022**, *9*, 20270–20281. [CrossRef]
110. Lu, H.; Jiang, M.; Cheng, J. Deep learning aided robust joint channel classification, channel estimation, and signal detection for underwater optical communication. *IEEE Trans. Commun.* **2020**, *69*, 2290–2303. [CrossRef]
111. Li, X.; Hu, X.; Zhang, R.; Yang, L. Routing protocol design for underwater optical wireless sensor networks: A multiagent reinforcement learning approach. *IEEE Internet Things J.* **2020**, *7*, 9805–9818. [CrossRef]
112. Weng, Y.; Pajarinen, J.; Akrour, R.; Matsuda, T.; Peters, J.; Maki, T. Reinforcement learning based underwater wireless optical communication alignment for autonomous underwater vehicles. *IEEE J. Ocean. Eng.* **2022**, *47*, 1231–1245. [CrossRef]
113. He, Z.; Shen, H.; Xu, W.; Zhao, C. Low-Cost Passive Beamforming for RIS-Aided Wideband OFDM Systems. *IEEE Wirel. Commun. Lett.* **2022**, *11*, 318–322. [CrossRef]
114. Zhang, Y.; Venkatesan, R.; Dobre, O.A.; Li, C. Efficient Estimation and Prediction for Sparse Time-Varying Underwater Acoustic Channels. *IEEE J. Ocean. Eng.* **2020**, *45*, 1112–1125. [CrossRef]

115. Abdallah, A.; Celik, A.; Mansour, M.M.; Eltawil, A.M. Multi-Agent Deep Reinforcement Learning for Beam Codebook Design in RIS-Aided Systems. *IEEE Trans. Wirel. Commun.* **2024**, *23*, 7983–7999. [CrossRef]
116. Qiao, Y.; Niu, Y.; Han, Z.; Mao, S.; He, R.; Wang, N.; Zhong, Z.; Ai, B. Joint optimization of resource allocation and user association in multi-frequency cellular networks assisted by RIS. *IEEE Trans. Veh. Technol.* **2023**, *73*, 826–842. [CrossRef]
117. Zuo, J.; Liu, Y.; Ding, Z.; Song, L.; Poor, H.V. Joint Design for Simultaneously Transmitting and Reflecting (STAR) RIS Assisted NOMA Systems. *IEEE Trans. Wirel. Commun.* **2023**, *22*, 611–626. [CrossRef]
118. Jan, Q.; Chao, Y.; Zhiwen, P.; Furqan, M.; Ali, Z.; Xiaohu, Y. Improved belief propagation decoder for LDPC-CRC-polar codes with bit-freezing. *China Commun.* **2024**, *21*, 135–148. [CrossRef]
119. Lin, Z.; Ni, Z.; Kuang, L.; Jiang, C.; Huang, Z. Dynamic Beam Pattern and Bandwidth Allocation Based on Multi-Agent Deep Reinforcement Learning for Beam Hopping Satellite Systems. *IEEE Trans. Veh. Technol.* **2022**, *71*, 3917–3930. [CrossRef]
120. Zhang, Y.; Mou, Z.; Gao, F.; Jiang, J.; Ding, R.; Han, Z. UAV-Enabled Secure Communications by Multi-Agent Deep Reinforcement Learning. *IEEE Trans. Veh. Technol.* **2020**, *69*, 11599–11611. [CrossRef]
121. Zhang, C.; Zhang, Z.-W.; Chen, Q.; Liu, L. Effect of hydrostatic pressure on the corrosion behavior of HVOF-sprayed Fe-based amorphous coating. *J. Alloys Compd.* **2018**, *758*, 108–115. [CrossRef]
122. Chen, L.; Duan, Y.; Cui, M.; Huang, R.; Su, R.; Qi, W.; He, Z. Biomimetic surface coatings for marine antifouling: Natural antifoulants, synthetic polymers and surface microtopography. *Sci. Total Environ.* **2021**, *766*, 144469. [CrossRef] [PubMed]
123. Parra, C.; Dorta, F.; Jimenez, E.; Henríquez, R.; Ramírez, C.; Rojas, R.; Villalobos, P. A nanomolecular approach to decrease adhesion of biofouling-producing bacteria to graphene-coated material. *J. Nanobiotechnology* **2015**, *13*, 82. [CrossRef]
124. 'LUMA', Hydromea. Available online: https://www.hydromea.com/underwater-wireless-communication (accessed on 19 April 2024).
125. Cong, L.; Srivastava, Y.K.; Solanki, A.; Sum, T.C.; Singh, R. Perovskite as a platform for active flexible metaphotonic devices. *Acs Photonics* **2017**, *4*, 1595–1601. [CrossRef]
126. Zhang, Y.; Zhang, J.; Renzo, M.D.; Xiao, H.; Ai, B. Performance Analysis of RIS-Aided Systems with Practical Phase Shift and Amplitude Response. *IEEE Trans. Veh. Technol.* **2021**, *70*, 4501–4511. [CrossRef]
127. Wang, J.; Shi, W.; Xu, L.; Zhou, L.; Niu, Q.; Liu, J. Design of optical-acoustic hybrid underwater wireless sensor network. *J. Netw. Comput. Appl.* **2017**, *92*, 59–67. [CrossRef]
128. Xiao, Z.; Yang, L.; Bithas, P.S.; Ansari, I.S.; Li, X.; Alouini, M.-S. Performance analysis of mixed underwater acoustic/optical relaying systems. *IEEE Trans. Wirel. Commun.* **2024**, *23*, 11357–11371. [CrossRef]
129. Zhou, Y.; Song, A.; Tong, F. Underwater acoustic channel characteristics and communication performance at 85 kHz. *J. Acoust. Soc. Am.* **2017**, *142*, EL350–EL355. [CrossRef] [PubMed]
130. Rudander, J.; van Walree, P.A.; Husøy, T.; Orten, P. Very-high-frequency single-input–multiple-output acoustic communication in shallow water. *IEEE J. Ocean. Eng.* **2018**, *44*, 943–955. [CrossRef]
131. Ahmed, R.; Mir, F.; Banerjee, S. A review on energy harvesting approaches for renewable energies from ambient vibrations and acoustic waves using piezoelectricity. *Smart Mater. Struct.* **2017**, *26*, 085031. [CrossRef]
132. Fang, L.H.; Rahim, R.; Fahmi, M.I.; Kupusamy, V. Modelling and Characterization Piezoelectric Transducer for Sound Wave Energy Harvesting. *J. Adv. Res. Fluid Mech. Therm. Sci.* **2023**, *102*, 81–98. [CrossRef]